

## Appendix E: Sensitivity Study

In addition to the main framework, a sensitivity study is conducted to evaluate the influence of the different parameters and modelling choices on the response of façade to settlement actions. The investigation refers to Façade 1, geometry variation A, placed on soil A, with standard masonry material, subjected to asymmetric hogging settlement (knick point at L/3) and soil-structure interaction stiffness based on Gazetas [26][31] (Figure E1). From this base model, one parameter at the time is varied and analysed. The following parameters are varied:

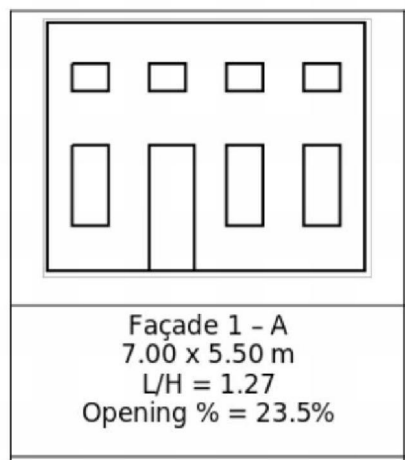
- soil-structure interaction stiffness: beside the original parameters calibrated from the Gazetas formulation [26][31], three additional set of stiffness are analysed, i.e. normal stiffness amplified and reduced by ten times. Additionally, the effects of the tangential stiffness is also investigated, by reducing it by 10 times. The results in terms of angular distortion against damage are presented in Figure E2. From the results it can be seen that the tangential stiffness has no effects on the final results and the model results independent from this parameter. The variation of the normal stiffness shows some differences in the façade behaviour. Large differences are detected in the applied settlement to reach the same amount of damage. A low stiffness softens the interaction between rigid supports and façade and a larger settlement amplitude is required to reach a similar damage of the model with original parameters. The stresses transmitted to the façade have a larger spread allowing the façade to damage for a higher angular distortion. Amplified value of normal stiffness shows more strict results in terms of applied angular distortion while the measured  $\beta$ . This stronger stiffness at the base reduces the ratio between measured and applied angular distortion to reach a specific damage (Figure E2). Just small differences are found between different soil-structure interaction stiffness.
- Façade mass: the original model and one with double façade mass are compared. The increment in mass does not lead to additional vulnerability. On the contrary, it shows a positive effect in terms of both measured and applied angular distortion. The plots are shown in Figure E3.
- Foundation type: in addition to the unreinforced masonry foundation, two variations where reinforced concrete foundation and no foundation are analysed. The difference between unreinforced and reinforced foundation is pretty large. The concrete strip largely improves the performance of the façade in terms of measured and applied angular distortion. The latter tends to a pretty large value to reach severe light damage. For this type of façade, the modelling of the unreinforced foundation has small effects on the final response of the façade to settlement. The  $\beta$ - $\Psi$  plot is shown in Figure E4.
- Façade stiffness: the effect of the façade stiffness on the settlement response is shown in Figure E5. In addition to the original stiffness (5 GPa), two variations

with reduced stiffness are considered. The reason of a reduced stiffness lays on the long term effects of the masonry material, also known as viscous-elasticity or creep-relaxation. This is based to the fact that the strain history affects the actual stress situation. This aspect is treated in the Eurocode 6 [35]. Equation 3.8 of the code provides a formulation for the long term stiffness, in order to allow creep effects. The stiffness is equal to the original stiffness divided by a creep factor (+1) depending on the material. For clay masonry the factor is equal to 0.7. The long term stiffness is then equal to 5 GPa divided by 1.7, which is equal to about 2.94 GPa. As additional variation, a value of 0.5 GPa is employed in order to consider a flexible, pre-damaged façade. The results clearly show the positive effects given by the reduced stiffness, which increase the measured angular distortion to damage the façade. On the other hand, the applied settlement to reach this damage is lower since the large flexibility allows the façade to reach a larger measured  $\beta$  earlier.

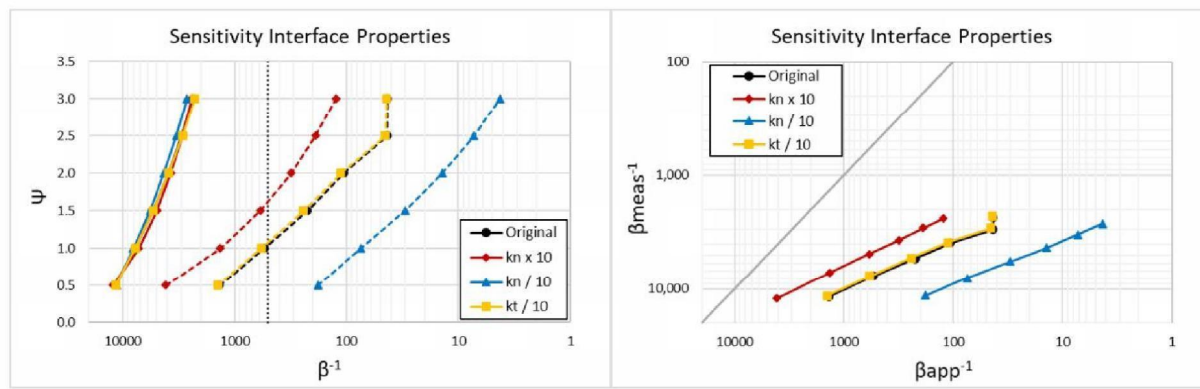
- Transversal walls: the interlocking effects provided by transversal walls at the two lateral edges is analysed. The two models represent a free standing façade where a damaged or poor interlocking with the transversal façades is present (no transversal walls) and a façade with a good interlocking (presence of transversal walls). The results, plotted in Figure E6, shows that the measured  $\beta$  is not influenced by the presence of the transversal wall, while it requires a lower applied settlement amplitude to reach a certain damage level when transversal walls are not present.

- Constitutive model: in addition to the orthotropic Engineering Masonry Model (EMM), the isotropic Total Strain Rotating Crack Model (TSRCM) is investigated. As already explained and shown in Appendix B, the TSRCM is quite vulnerable with respect to the EMM. This one has pre-defined direction (4: horizontal, vertical and two diagonal) for the cracks and each resistance is computed following different formulation which account for different strength. The TSRCM evaluates the cracking perpendicular to the principal stress directions. This causes a premature cracking and especially to an overestimation of the vertical cracking, which is treated quite differently with respect to the EMM (see Appendix B). The comparison between the two models in terms of  $\beta$ - $\Psi$  is shown in Figure E7.

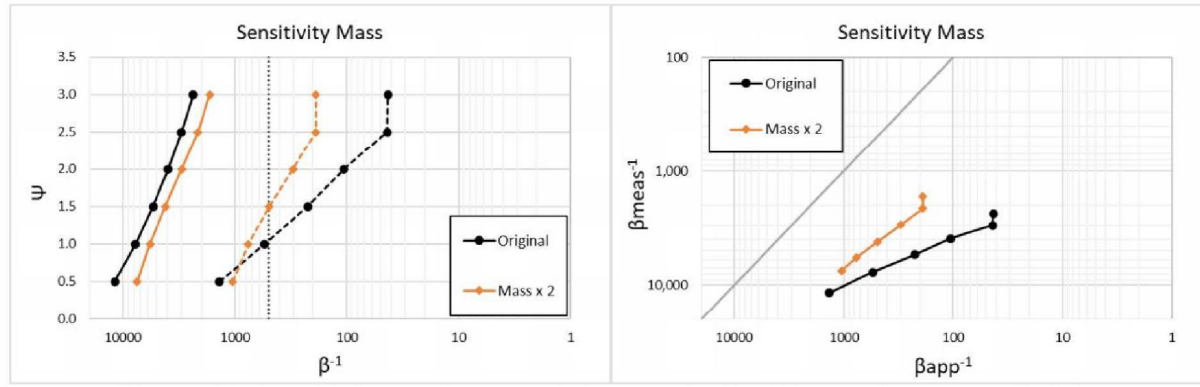
The overview of the  $\beta$ - $\Psi$  is summarized in Figure E8.



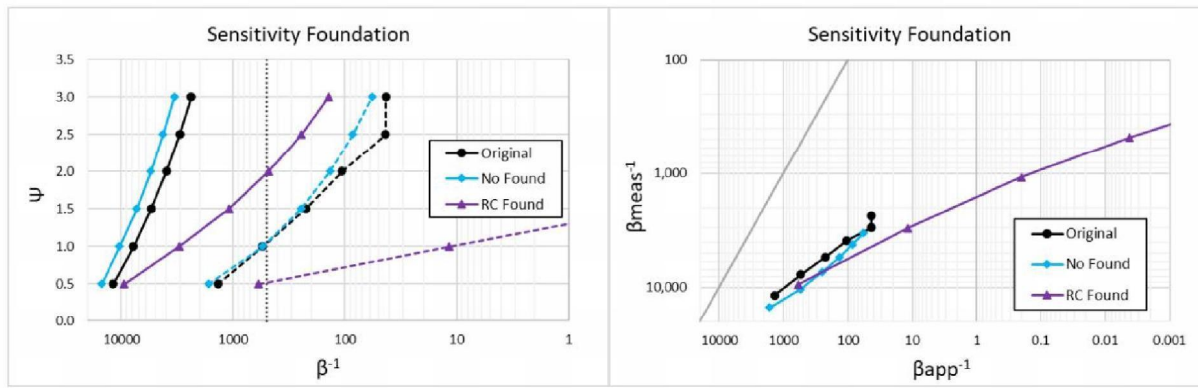
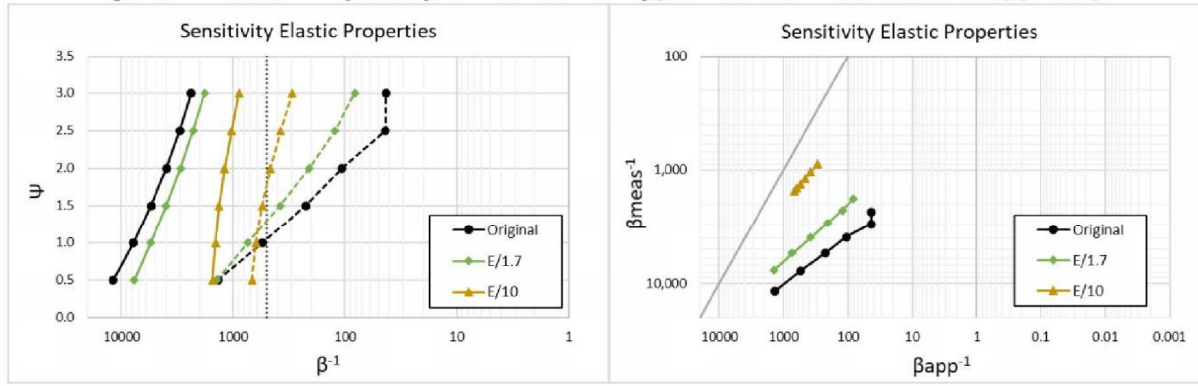
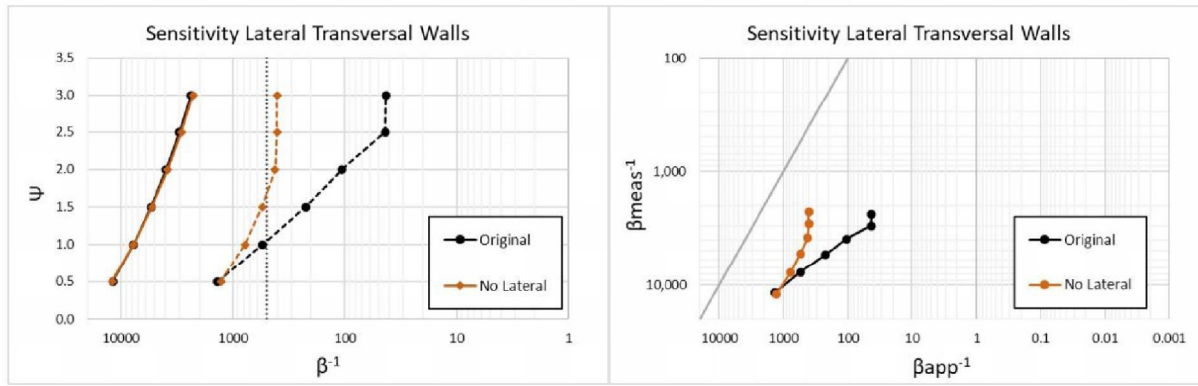
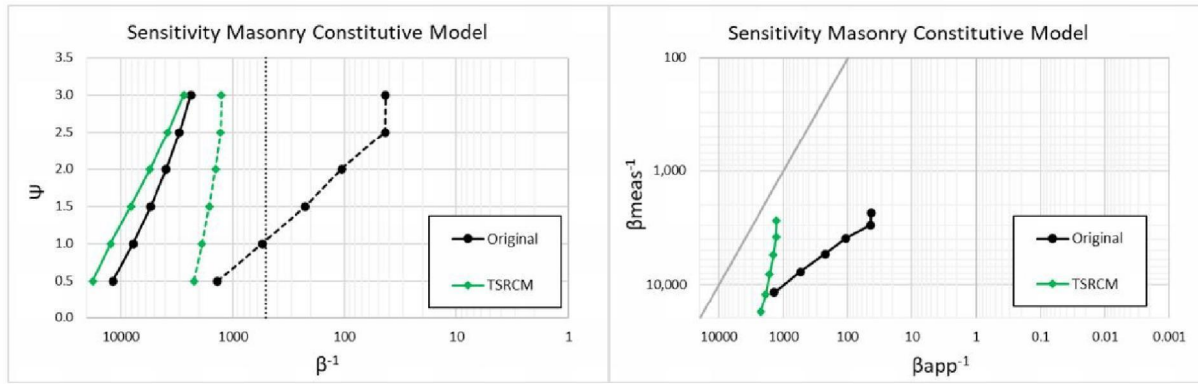
**Figure E1.** Façade 1, geometry A employed for the sensitivity study.



**Figure E2.** Sensitivity study on interface properties. Dashed lines refers to applied  $\beta^{-1}$ .



**Figure E3.** Sensitivity study on model mass. Dashed lines refers to applied  $\beta^{-1}$ .


**Figure E4. Sensitivity study on foundation type. Dashed lines refers to applied  $\beta^{-1}$ .**

**Figure E5. Sensitivity study on elastic properties. Dashed lines refers to applied  $\beta^{-1}$ .**

**Figure E6. Sensitivity study on lateral transversal walls. Dashed lines refers to applied  $\beta^{-1}$ .**

**Figure E7. Sensitivity study on masonry constitutive model. Dashed lines refers to applied  $\beta^{-1}$ .**

Variation	$\Psi=0.5$	$\Psi=1.0$	$\Psi=1.5$	$\Psi=2.0$	$\Psi=2.5$	$\Psi=3.0$	Variation	$\Psi=0.5$	$\Psi=1.0$	$\Psi=1.5$	$\Psi=2.0$	$\Psi=2.5$	$\Psi=3.0$
<b>Original</b>	11745	7720	5396	3925	3000	2363	<b>Original</b>	1367	542	223	106	43	43
<b>kn x 10</b>	12226	7201	4934	3697	2912	2410	<b>kn x 10</b>	4125	1340	587	313	189	124
<b>kn / 10</b>	11396	8034	5728	4292	3314	2662	<b>kn / 10</b>	180	75	30	14	7	4
<b>kt / 10</b>	11511	7720	5343	3886	2912	2270	<b>kt / 10</b>	1422	581	242	112	45	44
<b>Mass x 2</b>	7493	5728	4166	2970	2139	1668	<b>Mass x 2</b>	1045	760	490	301	189	189
<b>No Found</b>	14948	10306	7273	5450	4208	3347	<b>No Found</b>	1651	542	247	136	85	57
<b>RC Found</b>	9420	3030	1087	481	244	140	<b>RC Found</b>	587	12	0	0	0	0
<b>E/1.7</b>	7644	5450	3964	2941	2270	1788	<b>E/1.7</b>	1394	738	379	208	123	82
<b>E/10</b>	1525	1437	1327	1189	1034	882	<b>E/10</b>	674	623	547	462	375	295
<b>No Lateral</b>	11983	7720	5290	3809	2883	2270	<b>No Lateral</b>	1275	775	547	418	402	402
<b>TSRCM</b>	17733	12350	8114	5504	3809	2743	<b>TSRCM</b>	2226	1879	1619	1422	1275	1262

**Figure E8. Measured (left) and applied (right)  $\beta^{-1}$  values for different damage of the different analyses.**

## Appendix F: Weights for Probabilistic Counts

Material – follows normal distribution with 30% variance

Weak	0.25
Slightly weak	0.61
Standard	1
Slightly strong	0.61
Strong	0.25

Soil type – uniform distribution

Soil A	1.5
Soil B	1

Settlement Profile Shape – uniform distribution

Asymmetric Hogging	1
Symmetric Hogging	0.7

Soil-Structure interaction interface – correlated to soil type

High and soil A	1.5
Low and soil B	1.5
Original	1
High and soil B	0.7
Low and soil A	0.7

Profile Shape knick position – correlated to length of façade

Long Façade ( $L > \text{average}$ ) and Knick 4 or 5	2
Short Façade ( $L < \text{average}$ ) and Knick 4 or 5	0.5
Knick 2 or 3	1

**Geometric Properties** – see also Appendix K

- Length - Follows lognormal distribution  $\mu=1.482$  and  $\sigma=0.677$ 
  - o Example: a wall 3 m long is twice as likely (is more present in the data) than a wall of 6 metres.
- Height - Follows a non-parametric distribution fit to the data with a spacing of 0.5 metres. Alternatively, a lognormal distribution may be used with  $\mu=1.282$  and  $\sigma=0.428$ .
- L/H - Follows lognormal distribution  $\mu=0.321$  and  $\sigma=0.596$ 
  - o Example: A ratio of 1 (square wall) is twice as likely than a ratio of 2 (long wall).

### **Other Geometric properties**

Opening Ratio, Opening type - not defined from statistical data

## Appendix G: Empirical-based fragility curves

The empirical fragility curves presented in this work are based on a sample of 386 masonry buildings over different Dutch provinces recorded during different survey campaigns, 122 of which rest on shallow foundations and 264 on piled foundations.

Particularly, the damage and foundation information of 262 cases were retrieved from a cluster of masonry buildings in a neighbourhood of Schiedam from Peduto et al., [G.1], jointly with the available bed-joint measurements from an in-situ campaign carried out during the year 2003, a decade earlier. The field surveys include: i) the measurements of bed-joint levelling along the buildings' walls, ii) the documental information of the damage recorded via field survey, iii) the recorded foundation system (i.e. shallow or deep foundation).

The masonry buildings were manually classified according to four typologies proposed in [G.2], based on the structural features and the adjacency with other structures:

- Unit House (UH), refers to freestanding houses, (e.g. a single detached house) with an independent foundation system.
- Block Unit Single (UBHS), refers to a single building part of an homogeneous block (e.g. a single address of a block of row houses, or a semi-detached house).
- Block Unit Multiple (UBHM), refers to an homogeneous building block, with the same foundation system (e.g. a block of row houses).
- Others (OTH), refers to cases not classified in the previous 3 categories (e.g. sheds or warehouses).

A summary of all the available information is proposed in Table G.1 in relation to their location (province).

**Table G.1. Summary of building data distinguished by location, building typology, foundation type and damage level.**

Province	Foundation type		Building typology				Year of construction (y)			
			190	195	0	0	< y	< y	200	y > 2000
	Shallow w	Deep p	U H	U B H S	U B H M	O T H	y ≤ 1900	< y ≤ 195	200	y > 2000
<b>South-Holland</b>	83	206	0	27	262	0	0	289	0	0
<b>North-Holland</b>	2	18	3	11	4	2	3	6	11	0
<b>Utrecht</b>	25	38	44	5	3	11	11	15	34	3
<b>Other</b>	12	2	11	1	0	2	0	10	4	0
<b>Total</b>	122	264	58	44	269	15	14	320	49	3

The buildings were divided into three groups based on the visible damage: i) "undamaged cases" refers to cases with no significant observable damage, ii)

"light damage" refer to aesthetic damage characterized by very fine/fine crack up to 5 mm and iii) "moderate to severe damage" implies severe and very severe damage that could be associated with a risk for the structural safety. The collected bed-joint levelling measurements of each building allowed tracing back the displacement profile assumed to correspond to the resulting settlement profile at foundation level. Thus, the measured relative rotation, selected as representative of the intensity of the settlement causing damage on buildings, was computed for each case.

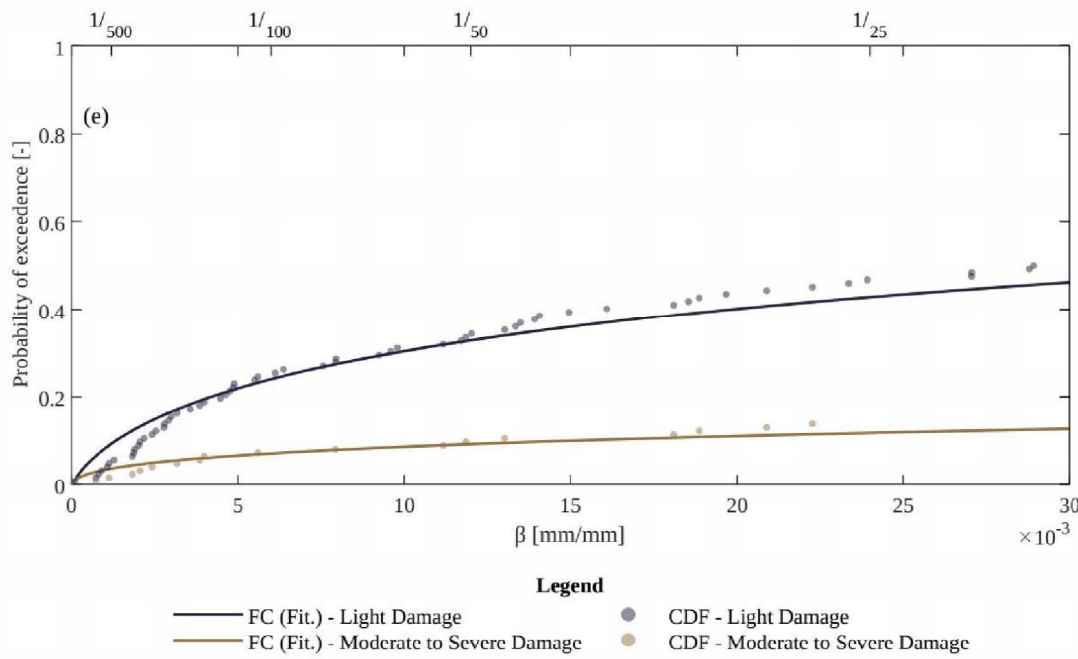


**Figure G1. Fragility curves generated for the relative rotation  $\beta$  for building resting on shallow foundations.**

The cumulative density functions are obtained by counting the number of buildings reaching or exceeding each damage state (i.e., "light damage" and "moderate to severe damage"), in relation to the total number of cases. The fragility curves were then derived by fitting a lognormal distribution to the cumulative density functions.

Additional analyses were carried out to investigate the shapes of the settlement displacements for the building's dataset, based on the bed-joint levelling measurements.

Accordingly, each profile was sorted as one of the eight proposed shapes. Among the classified settlement shapes, Figure G.2. and Figure G.3. shows how the most recurrent profiles, associated with both deformation and an overall tilt, are more frequent than the profiles without tilt. This agrees with the observation in the study of Charles and Skinner [G.2], that states "*In most practical situations, settlement will cause both distortion and tilt*" referring to sagging and hogging profiles with a non-uniform tilt.

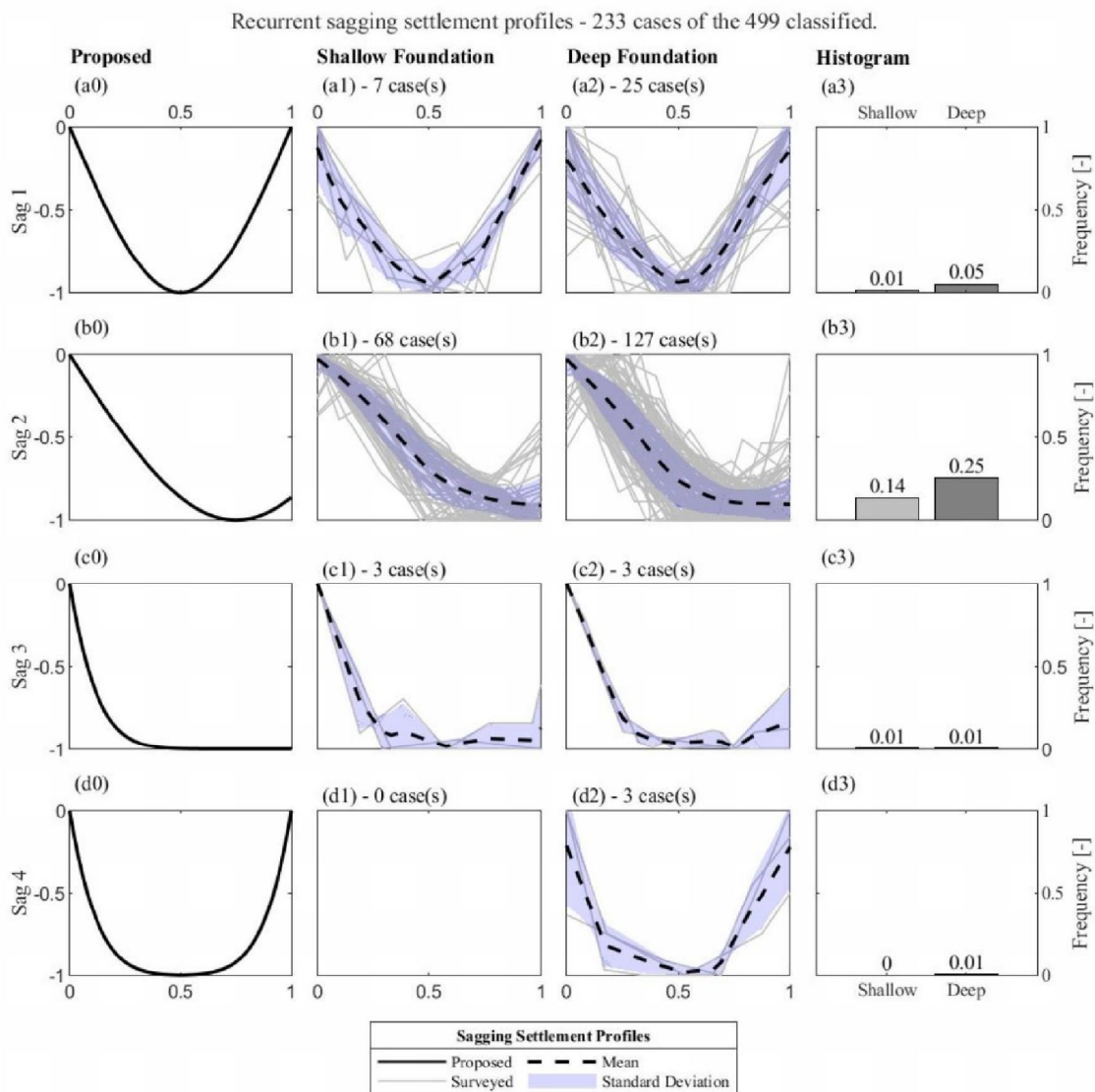


**Figure G2. Nondimensional sagging settlement profiles of the considered surveyed buildings:** from (a0) to (d0) Proposed settlement profiles; Settlement profile for: from (a1) to (d1) for buildings on shallow foundations, and from (a2) to (d2) for buildings on deep foundations. The number of cases for each foundation system is indicated on top of each bin from (a3) to (d3).

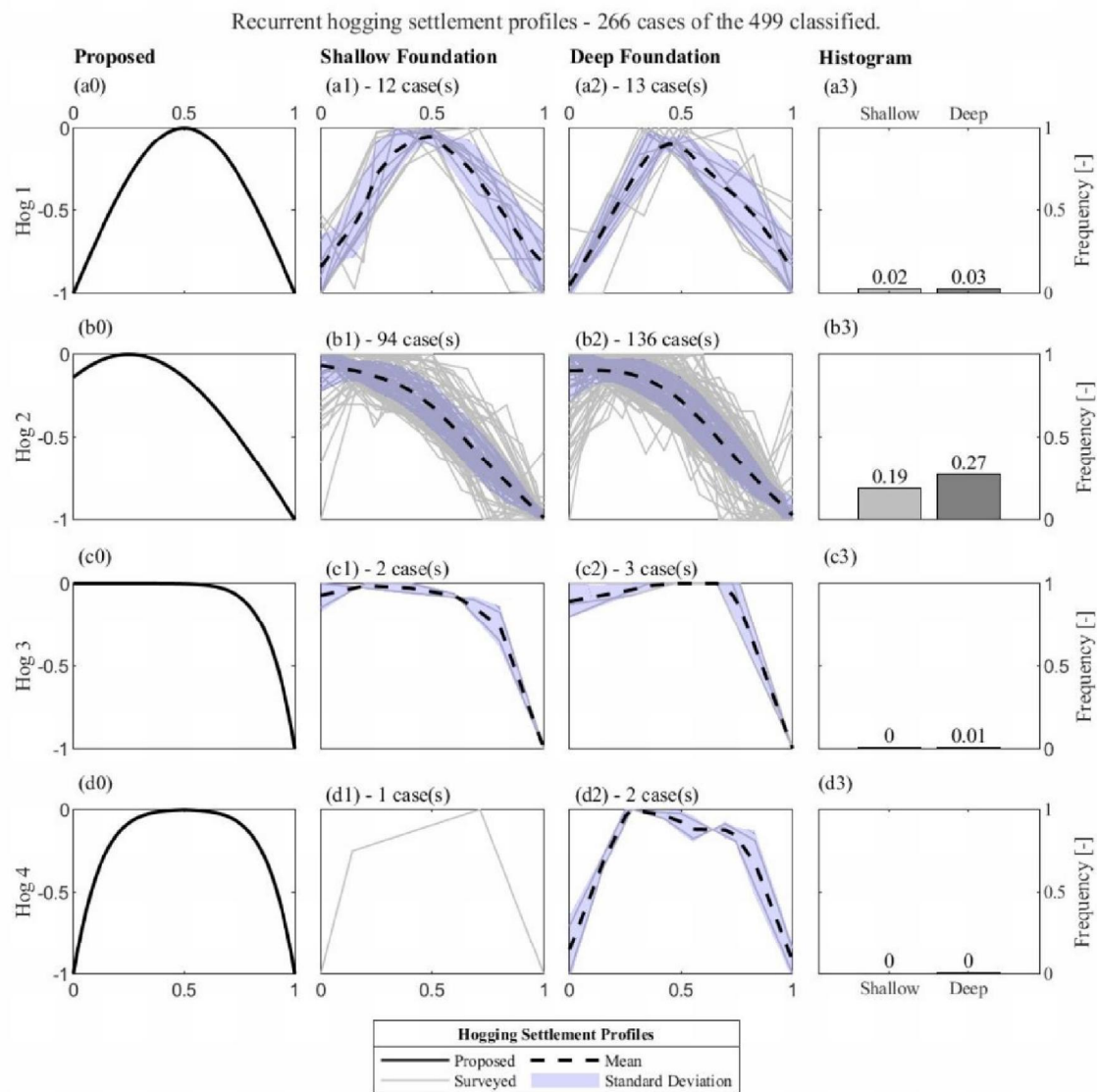


**Figure G3. Nondimensional hogging settlement profiles of the considered surveyed buildings: from (a0) to (d0) Proposed settlement profiles; Settlement profile for: from (a1) to (d1) for buildings on shallow foundations, and from (a2) to (d2) for buildings on deep foundations. The number of cases for each foundation system is indicated on top of each bin from (a3) to (d3).**

It should be highlighted that the sampling technique, the way the building surveys were collected, is not a random sample (in which every building in the Netherlands would have the same probability of being picked for the analysis), but a convenience sample (which means that the sample was collected with what was close at hand, so buildings already surveyed, with damage claims etc.). Other studies have made use of a sample of buildings that can be defined as convenience sample (e.g., Peduto et al. [G.1] with about 700 buildings and their fragility curves); this means that the conclusions are not easily generalizable for the entire building stock in the Netherlands.

Although this sampling approach is rapid and cost-effective, it is indeed characterized by sampling errors and bias that cannot be measured. In fact, it

is also defined as a type of “non-probability” sample due to the difficulty to generalize the conclusion to the entire population. Nevertheless, they are often used for qualitative and exploratory studies.

In sum, the level of masonry bed-joints, assumed to have been built perfectly horizontal, has been used to decipher settlement deformations on the walls of buildings; these measured profiles reveal that asymmetric hogging or sagging, where only one corner of the wall or building settles, and including general building tilt, are the most common settlement shapes.

### References

- [G.1] Peduto, D., Korff, M., Nicodemo, G., Marchese, A., Ferlisi, S. (2019). Empirical fragility curves for settlement-affected buildings: Analysis of different intensity parameters for seven hundred masonry buildings in The Netherlands. *Soils and Foundations* 59, 380-397, doi:10.1016/j.sandf.2018.12.009.
- [G.2] Charles, J. A., Skinner, H. D. (2004). Settlement and tilt of low-rise buildings. *Proceedings of the Institution of Civil Engineers-Geotechnical Engineering* 157, 65-75.
- [G.3] (UNDER REVIEW) Prosperi, A., Korswagen P. A., Korff M., Schipper R., Rots J.G., Empirical fragility and ROC curves for masonry buildings subjected to settlements.

## Appendix H: Sagging Settlement Profiles

In the main report, four settlement profiles are selected, two symmetric and two asymmetric profiles with different knick points. The employed settlement profiles are all hogging profiles. This choice follows field data (see Appendix G), which shows that hogging profiles are the most common ones found in the inspected cases. A sensitivity study where two sagging settlement profiles are modelled underneath four façades (Façade 1, 2, 3 and 4) is herein conducted. The two sagging profiles are produced by flipping the two hogging settlements. The four settlement profiles (calibrated on Façade 1) are shown in Figure H1. This sensitivity study is in addition to the existing parameters varied in Appendix E and warrants a separate discussion.

The results in terms of  $\beta\text{-}\Psi$  of Façade 1 subjected to the four types of settlement are reported in Figure H2. The data points are also plotted in a graph where applied and measured angular distortions are compared (Figure H2). The curves show that the angular distortion measured at the base of the façade for all damage points is lower for the two hogging cases. On the contrary, the façade gets damaged for reduced values of applied settlement. The ratio between measured and applied angular distortion reduces as well. This additional vulnerability is strictly correlated to the façade geometry. When the middle portion sags, the top bed-joint of the pier between door and window opens up (Figure H3). Additional flexural cracks in the more flexible central part of the façade also appear pretty early in the settlement stage. Moreover, the portion of façade mobilized by the sagging action is much higher than the corresponding hogging settlement (Figure H1).

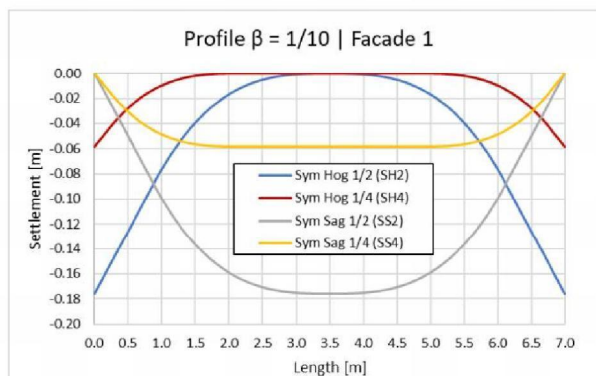


**Figure H1. Hogging and Sagging settlement profiles applied to the model of Façade 1.**

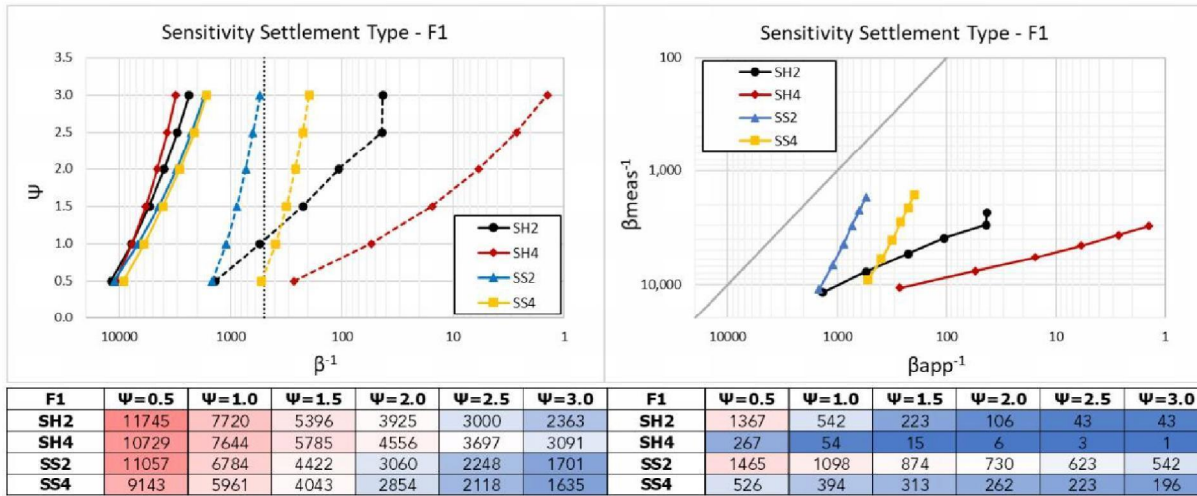


**Figure H2. Sensitivity study on settlement profiles for Façade 1.** Dashed lines refers to applied  $\beta$ . Measured (left) and applied (right)  $\beta^{-1}$  values.

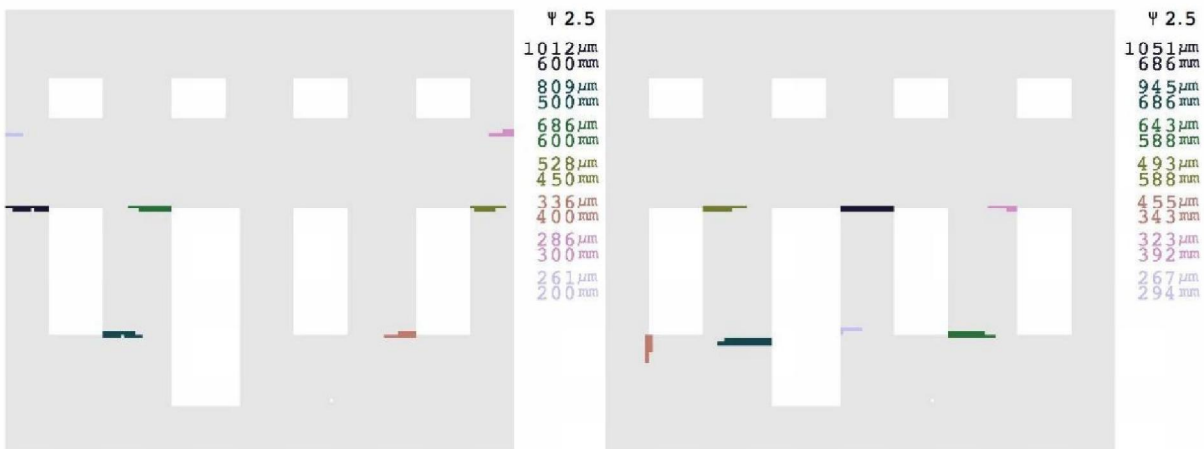


**Figure H3. Crack pattern of Façade 1, subjected to hogging SH2 (left) and sagging SS4 (right).** Cracks at DS2.

When analysing the results of the long Façade 2, it can be seen how the failure mechanism shifts from a brittle vertical cracking starting from the top of the façade to a flexural mechanism involving the piers at the right side of the façade (Figure H5). The top part of the façade when sagging is applied is entirely in compression. The tension part now shifts to the stiffer foundation which is able to better adapt to the deformation without showing brittle vertical cracking. The plots in Figure H4 show that the hogging settlement is still the most critical for Façade 2. Both applied and measured settlement at certain damage is still the lowest for hogging settlement (SH2). The measured-applied  $\beta$  ratio of SH2 and SS2 is pretty similar.

A similar shift in the failure mechanism is also detected in Façade 3. Here the vertical cracks below the window, typically found during hogging settlement, are replaced by horizontal flexural cracks starting at window corners (Figure H7). Damage is mainly located at ground floor in the central pier. Plots of  $\beta$ - $\Psi$

are shown in Figure H6. The two models with hogging settlement are still the most critical in terms of measured and applied angular distortion.

Façade 4 results are summarized in Figure H8. The crack pattern due to hogging and sagging settlement actions is depicted in Figure H9. The failure when hogging deformations are applied is concentrated at the top of the façade, where vertical cracking extends from the top edge to the window corner due to limited spandrel height. Masonry spandrels result in compression when sagging actions are applied. In this case, diagonal shear cracks in the window banks are detected at the two lateral sides of the façade. An horizontal flexural crack is also detected at the top of the left pier of the mid window. Similar to the other long façade (Façade 2), Façade 4 presents more vulnerability to hogging actions rather than sagging actions.

In conclusion, most façades are more vulnerable to hogging settlement actions in terms of both measured and applied settlement. Only Façade 1, due to its large opening area in the middle of the façade, shows damage for lower sagging settlement amplitude with respect to the hogging settlement. This is mainly correlated with the geometry of the façade and to the fact that the imposed sagging actions deform a larger portion of the façade. Due to the limited observation of these settlement profiles in the field (Appendix G) the hogging settlement is still considered the best option to characterize the behaviour of masonry façades to vertical base deformation and represents a conservative variation when selecting only one type of settlement profile.

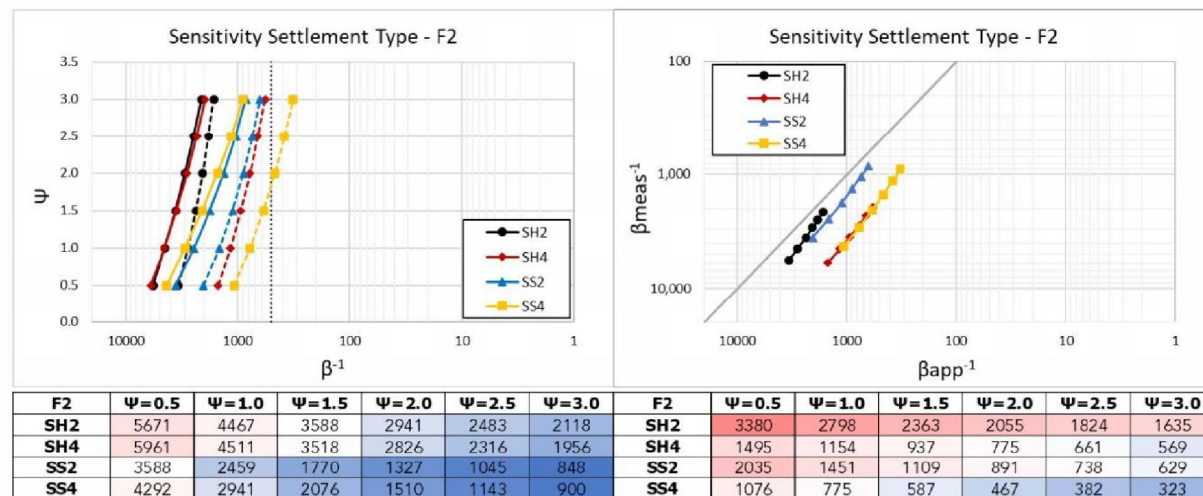


**Figure H4. Sensitivity study on settlement profiles for Façade 2. Dashed lines refers to applied  $\beta$ . Measured (left) and applied (right)  $\beta^{-1}$  values.**

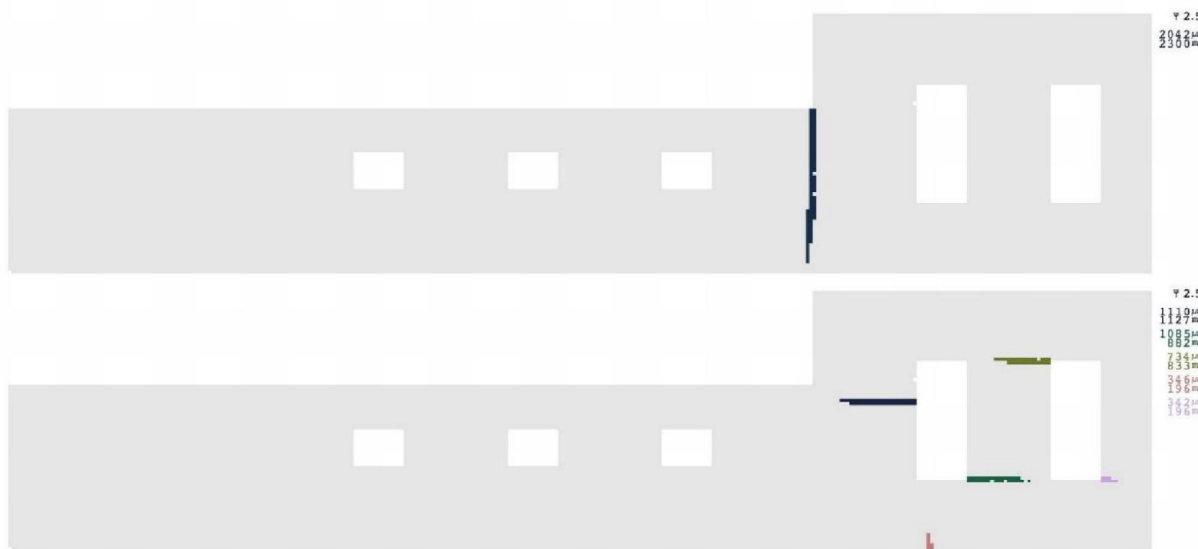


**Figure H5. Crack pattern of Façade 2, subjected to hogging SH2 (left) and sagging SS4 (right). Cracks at DS2.**

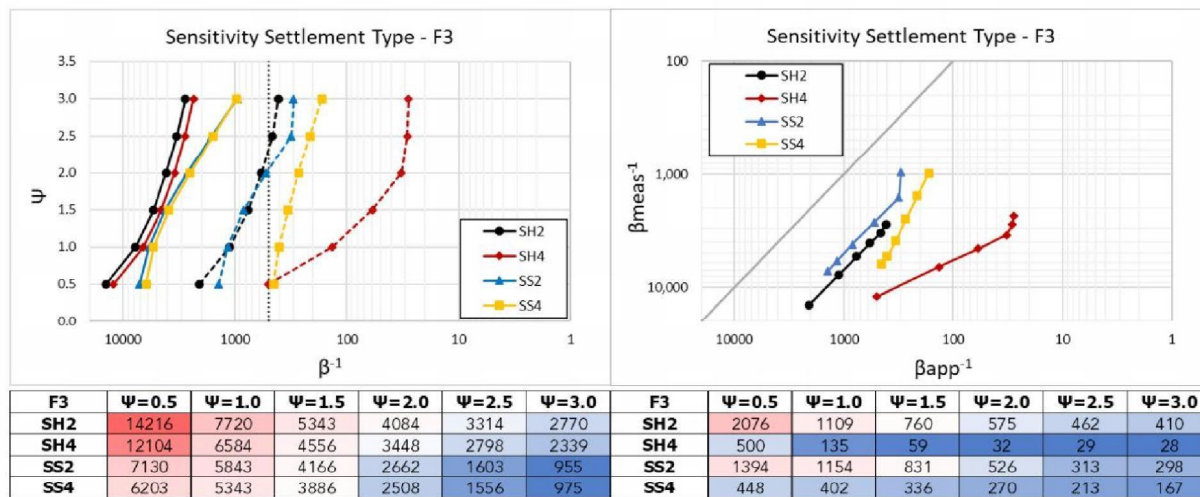


**Figure H6. Sensitivity study on settlement profiles for Façade 3. Dashed lines refers to applied  $\beta$ . Measured (left) and applied (right)  $\beta^{-1}$  values.**

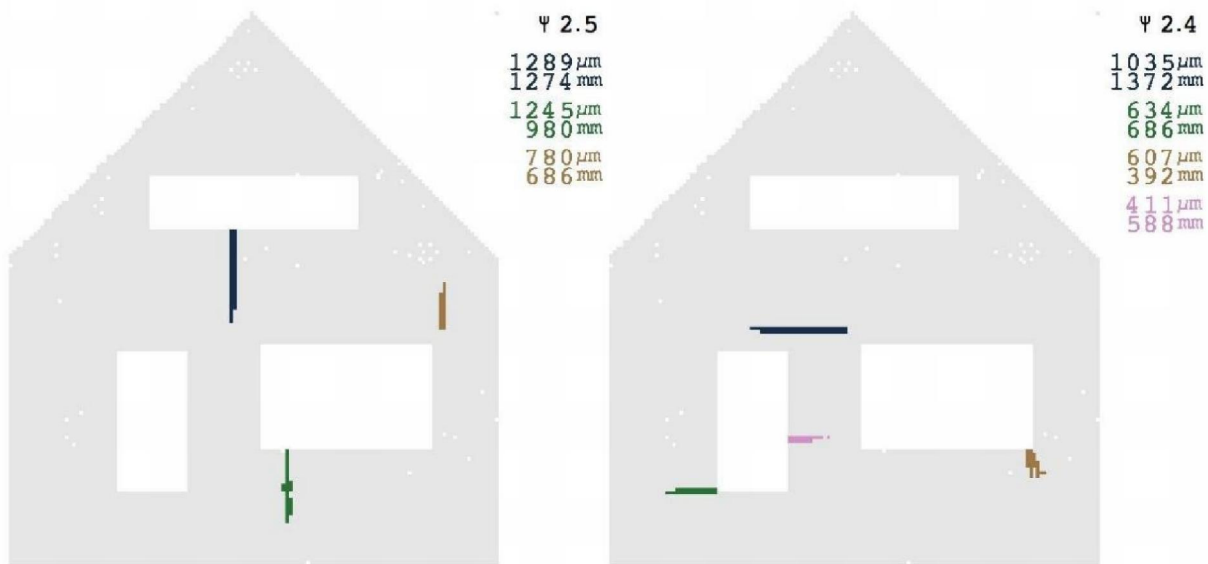


**Figure H7. Crack pattern of Façade 3, subjected to hogging SH2 (left) and sagging SS4 (right). Cracks at DS2.**

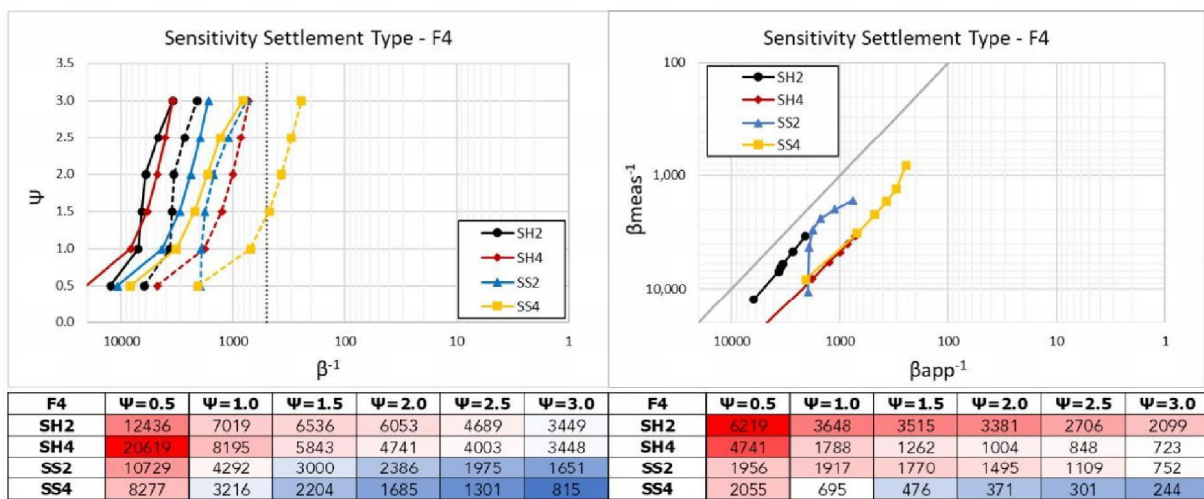


**Figure H8. Sensitivity study on settlement profiles for Façade 4. Dashed lines refers to applied  $\beta$ . Measured (left) and applied (right)  $\beta^{-1}$  values.**





**Figure H9. Crack pattern of Façade 4, subjected to hogging SH2 (left) and sagging SS4 (right).  
Cracks at DS2.**

## Appendix J: Model for Beta-Psi Extrapolation

Several of the FEM models did not reach high values of Psi and several other models exhibited small jumps in Psi when the applied beta was smoothly increased due to the cracking behaviour and the solving algorithms employed in the (material) models. These issues can be mitigated by utilising a model function that follows the relationship between the distortion beta and  $\Psi$ , smoothing out small jumps and continuing its trend past the largest values of  $\Psi$  obtained in the models. Figure J1 shows an example of the model function in action.

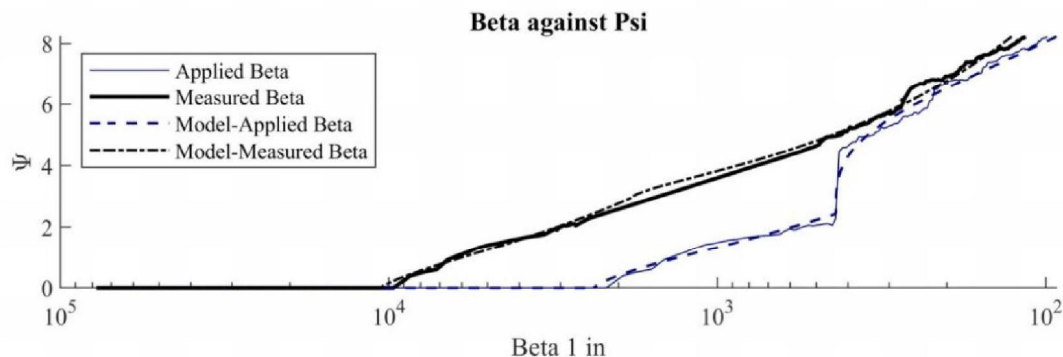


Figure J1. Example of model function fit to the computed result of  $\Psi$  against the applied and measured distortions. The three parts of the functions can be identified.

Equation J1:

$$f(x) = \begin{cases} 0 & x \leq x_0 \\ c_1 + a_1 \cdot (x - x_0)^{b_1} & x_0 < x \leq x_3 \\ f_{x_3} + a_2 \cdot (x - x_3)^{b_2} & x_3 < x \end{cases}$$

$$f_{x_3} = f(x_3)$$

$$x_0 := \Psi(\min|x|) > 0$$

$$x_3 := \Psi(\min|x|) \geq 3$$

The model function,  $f(x)$  as presented in Equation J1, is defined for three discontinuous intervals. Before a value  $x_0$ , the fit returns zero;  $x_0$  corresponds to the lowest beta value in the original data for which  $\Psi$  is no longer zero. Similarly,  $x_3$  determines the lowest beta for which  $\Psi$  is 3; when a value of 3 is not reached in the data, the  $x_3$  identifies the last beta value in the data. For beta ( $x$ ) between  $x_0$  and  $x_3$ , the function returns a power law with regression coefficients  $a_1$ ,  $b_1$ , and  $c_1$ . For  $x$  above  $x_3$ , another power law, with a different slope and shape to accommodate the damage behaviour beyond  $\Psi=3$ , continues the fit; this second power law continues from the same point ( $x_3$ ,

$f(x_3)$  and employs coefficients  $a_2$  and  $b_2$ . The model function has thus five regression coefficients.

The smoother function, capable of extrapolating beyond the domain of the original data, is used in the simulations for the fragility curves.

## Appendix K: Wall geometries from BAG 3D

"3D BAG is an enhanced version of the Dutch Basisregistraties Adressen en Gebouwen (BAG) data set, with added height information. The 3D BAG is created and maintained by the 3D geoinformation research group at the Delft University of Technology" [2]. This data set is freely available and contains several fields of interest for every building; specifically, the geometry, including the height of the buildings, has been determined from a point cloud of aerial (laser) measurements. The reader is referred to the interactive version [3]; see Figure K1.

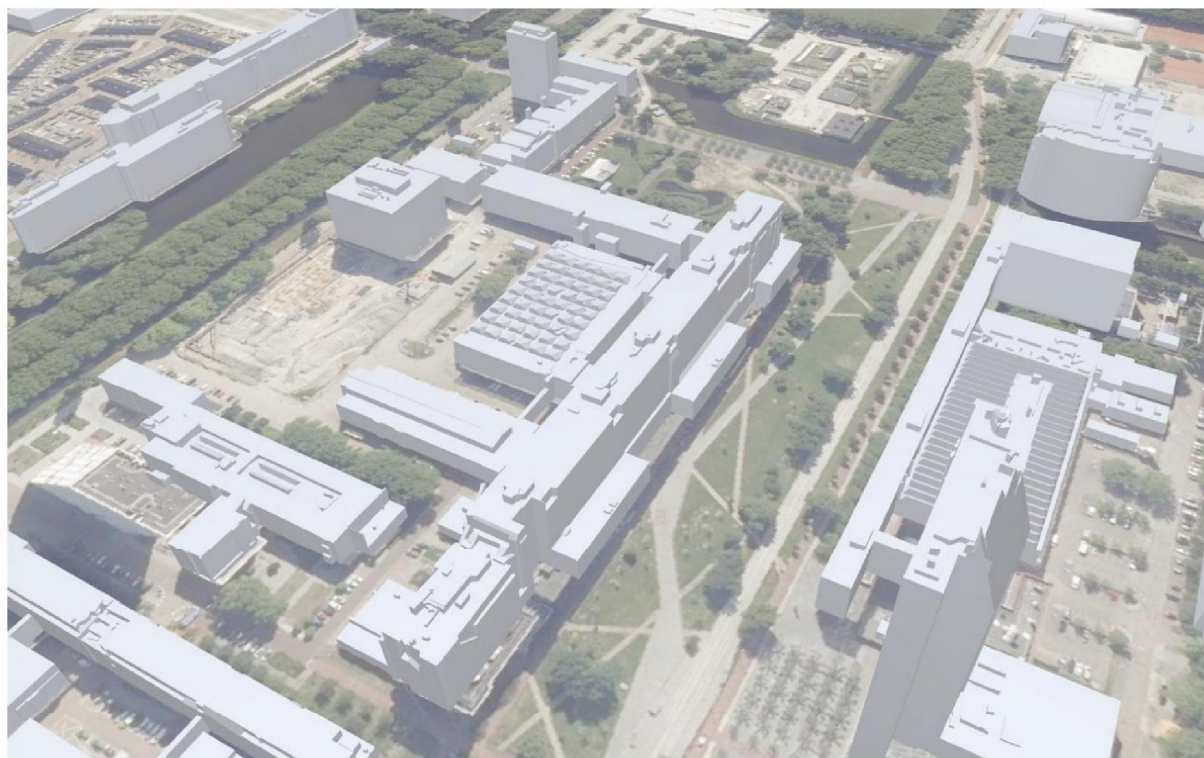


Figure K1. 3D view of the faculty of Civil Engineering and Geosciences on the campus of the TU Delft projected onto an aerial view of the ground. From the website of 3dbag.nl [3].

For this study, the entire database has been downloaded and post-processed so as to obtain statistics about the shape of buildings' walls and other building properties, such as slanted roofs, variable roof height, etc. About 45GB of data is present in the Postgres SQL database; from this data, information about 8 million buildings, constructed across the Netherlands between 1900 and 1999, has been extracted. The geometry data encoded with the PostGIS plugin for SQL was converted and imported into Matlab such that building geometry could easily be visualised and processed into statistics at a building population scale. Figure K2. shows a histogram of the buildings according to their construction

year. The influence of historic events, such as WW2, and uncertainty in the data, such as guesses about the construction year being rounded to the nearest decade, are visible in the graph.

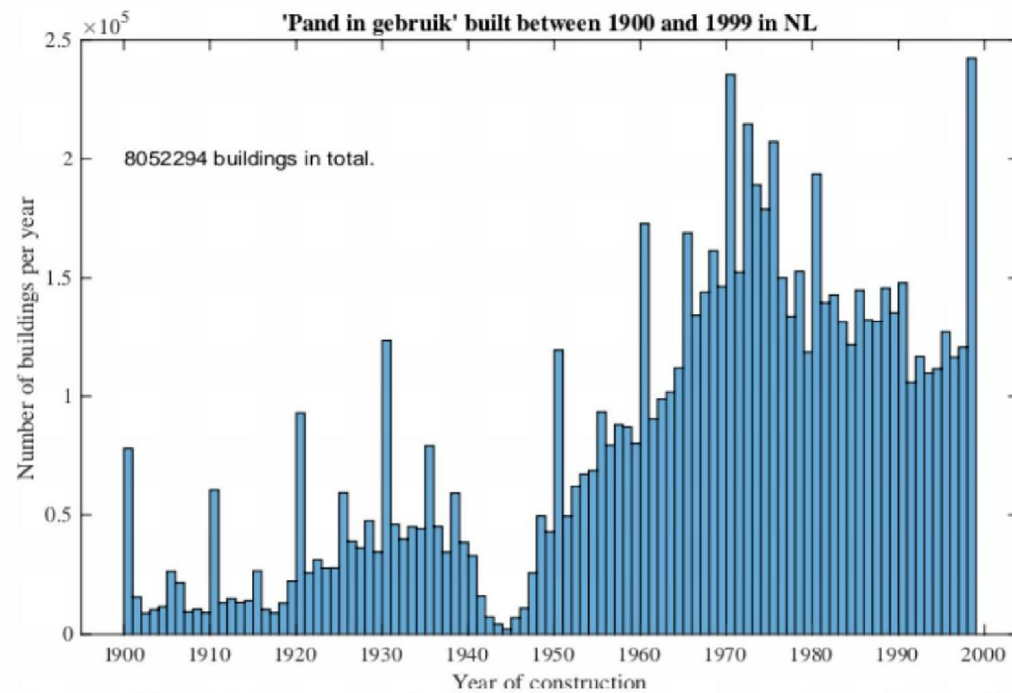


Figure K2. Histogram of the year of construction for buildings in the Netherlands available in the BAG 3D database.

The geometry of the buildings was further processed to identify individual façades in the buildings. A purposely-written program ‘unfolds’ the 3D geometry into a paper-like net by reconstructing the façades’ shape from the roof geometry. Imperfections in the original geometry are restored to produce clearly-defined façades, identifying what could be individual walls. Figure K3 presents two exemplary results from the unfolding program. The algorithm determines thus the wall height and length as well as the overall shape of each wall.

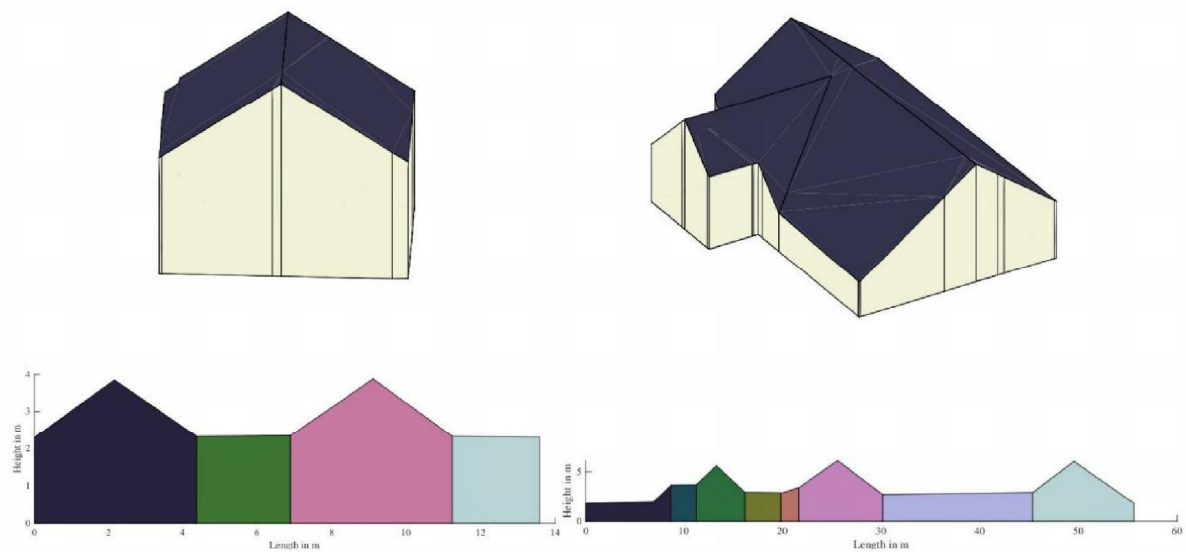


Figure K3. Two examples of the unfolded geometry of two buildings showing the individual walls' length and height.

Approximately 150 thousand building geometries, within the province of Groningen, were successfully interpreted with the unfolding program. This was deemed a sufficiently large sample size to obtain statistical data about the trends of building wall shape. Figure K4 reveals that walls typically have a length between 2 and 10 metres with longer walls being increasingly less common. Similarly, wall height peaks at 2.8 and 5.7 metres, corresponding to a single or double storey house; wall heights between 2 and 7 metres are thus common, with the latter probably belonging to the attic of a gable-roof, two storey house. However, it is outside of the goal of this study to attempt to define typologies or sub-typologies from the geometry data; instead, only wall dimensions and shape are of interest and can be reliably obtained. The length and height of the walls can be used to determine a ratio which is critically influential when predicting settlement-related damage. The bottom graph in Figure K4 shows how the typical length/height ratio varies between 0.5 and 2.5. This means that 'long' façades, with ratios around 4, are comparatively uncommon.

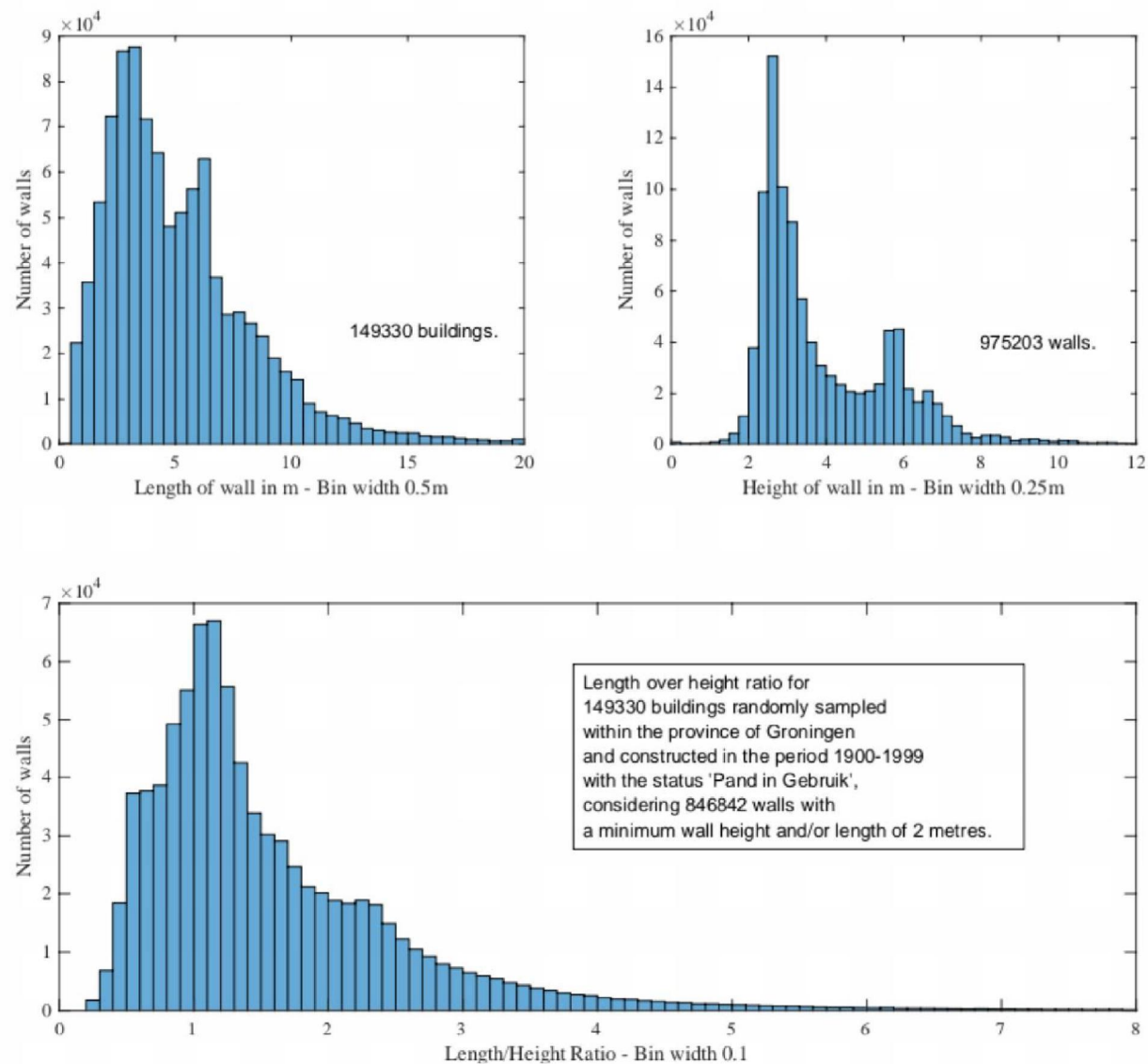


Figure K4. Wall length and height.

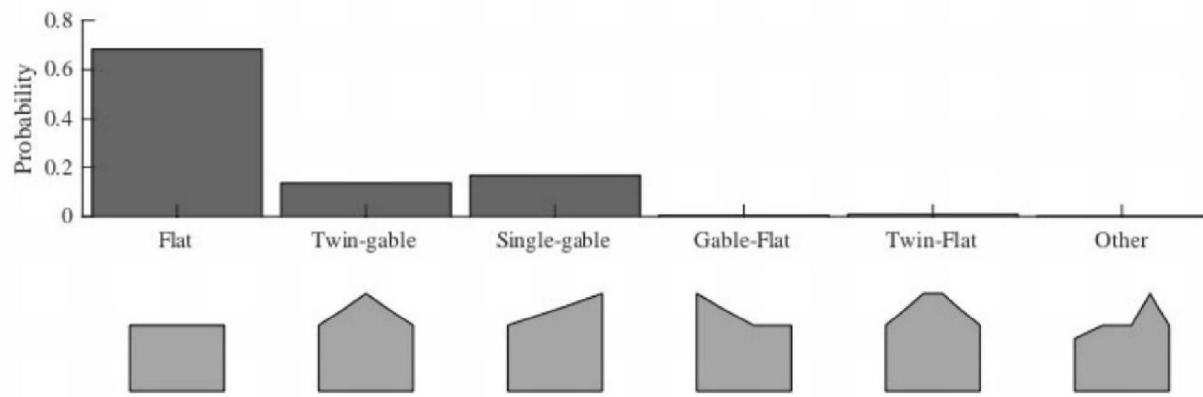


Figure K5. Wall-shape categories automatically assigned for the 847 thousand walls (see Figure K4).

Furthermore, the walls for which the length/height ratio was determined, were also automatically categorised based on their shape as illustrated in Figure K5. Five typical shapes were formulated which encompass most wall geometries. Note that these do not identify the roof shape of the buildings but of the individual walls. Consequently, the most common wall shape is that with a flat upper side which is present in buildings with flat roofs as well as on the sides of buildings with gable roofs. Moreover, two single-gable walls, which may not appear precisely on the same plane or may be separated by a chimney, may be present to form a twin-gable roof.

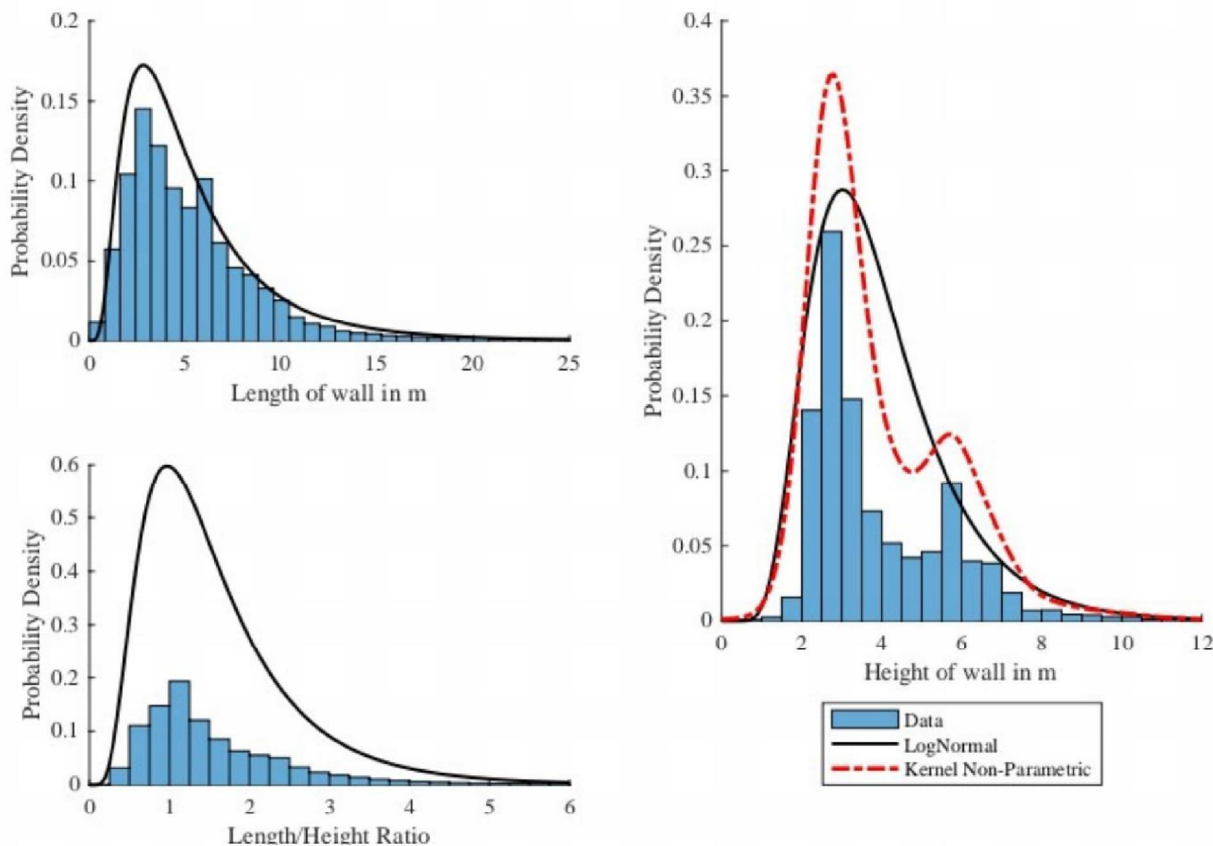


Figure K6. Distribution fit to length and height properties.

The statistics of the geometrical properties obtained from the data can be represented with fitted distributions. The spread of the data matches well with the shape of a lognormal distribution in all cases; however, for representing the height, because of the peak corresponding to walls of two storeys high, either a double lognormal distribution or a non-parametric distribution would better represent the data. In this case, a Kernel distribution can be used to characterise the wall height. The parameters of the lognormal distributions can be found in Table K1.

Table K1. Parameters for the lognormal fits.

Name	Mu	Sigma
Length	1.470	0.663
Height	1.282	0.421
Length/Height Ratio	0.308	0.580

An initial attempt at characterising the building data was conducted with only 48 thousand geometries, instead of the 150 thousand geometries processed later. The change in the mu and sigma values of the fitted distribution was almost negligible (with the largest value being below 4% and in most cases

below 1%). This means that a larger sample size (or the entire building population) is unnecessary to characterise the wall geometry. In fact, 207 thousand buildings were available within the Groningen region in the 3D BAG database; but the database is updated continually and it does not include all buildings (with sheds and small buildings excluded) so it cannot be said with certainty what the entirety of buildings is. Nevertheless, the sample size selected herein is deemed sufficiently large.

The analysis of BAG 3D has provided insight into relevant wall shape, length, and height. This insight can be employed when elaborating FEM model geometries or interpreting their results. Nevertheless, information about the wall openings and their distribution could not be obtained from this database.

#### References K

- [K.1] <https://docs.3dbag.nl/en/>
- [K.2] <https://tudelft3d.github.io/bag3d/intro.html>
- [K.3] <https://3dbag.nl/en/viewer>

# IEDB: Opscho nen contou rlijnen



Cascadeplein 10  
9726 AD Groningen

Antwoordnummer 3061  
8000 WB Zwolle

0800 44 44 111  
[contact@schadedoormijnbouw.nl](mailto:contact@schadedoormijnbouw.nl)

Onderwerp	: IEDB: Aanpak opschonen contourlijnen
Datum	: 9 september 2022
Portefeuillehouder onderwerp	: 5.1.2e
Contactpersoon (auteur)	: 5.1.2e 5.1.2e 5.1.2e
Doel (ter besluit/ter bespreking/ter kennisname)	: ter besluit

## 1. Aanleiding

Voor het analyseren van de Indirecte Effecten door de Diepe Bodemdaling (IEDB) is de bodemdaling benodigd. Omdat het IMG enkel verantwoordelijk is voor schade veroorzaakt door het Groningenveld en gasopslag Norg is de bodemdaling vanaf aanvang van de gaswinning benodigd ten gevolge van enkel deze activiteiten.

Het bepalen van de contourlijnen met de bodemdaling door het Groningenveld en gasopslag Norg is specialistisch werk en kan enkel worden verzocht door zogenaamde reservoirtechnologen. TNO is benaderd om de contourlijnen aan te leveren per 5 jaar vanaf de periode 1963 tot heden. TNO heeft aangegeven deze contourlijnen te kunnen leveren niet eerder dan Q4 (begin december 2022). Om toch verder te kunnen gaan met de IEDB-analyse zijn zogenaamde opgeschoonde contourlijnen gegeneerd. Het gehanteerde bronmateriaal, de procedure van opschonen en de mogelijke onnauwkeurigheden en bijbehorende consequenties worden in dit stuk beschreven.

## 2. Bronmateriaal

De NAM publiceert sinds 2000 eens in de 5 jaar een statusrapport met de bodemdaling door aardgaswinning door de NAM-gasvelden in Groningen, Friesland en het noorden van Drenthe. De in deze rapporten opgenomen contourlijnen met bodemdaling door de gaswinning worden samengesteld uit een combinatie van InSAR-satellietdata met gemeten maaivelddaling en berekende maaivelddaling uit reservoirmodellen op basis van geologische/reservoir-data aangevuld met winningsdata (hoeveelheid ontrokken gas per gasveld/winningsput en reservoirdrukken). Door resultaten onderling te correleren kan met de reservoirmodellen een betere prognose voor de toekomst worden afgegeven. De rapporten zijn altijd voorzien met prognoses van de bodemdaling tot 60 jaar na publicatie.



De door de NAM gepubliceerde contourlijnen met de bodemdaling eind jaren 1998, 2003, 2008, 2013 en 2018 zijn door TNO geverifieerd en vervolgens vrijgegeven en gebruikt als bronmateriaal.

Om inzicht te krijgen in de ligging van de kleine gasvelden en de zoutwinning is Veendam en Westerlee is gebruik gemaakt van het NLOG-portaal (Nederlandse Olie- en Gasportaal; <https://www.nlog.nl/bestanden-interactieve-kaart>).

In een later stadium zijn nog de volgende contourlijnen aangeleverd:

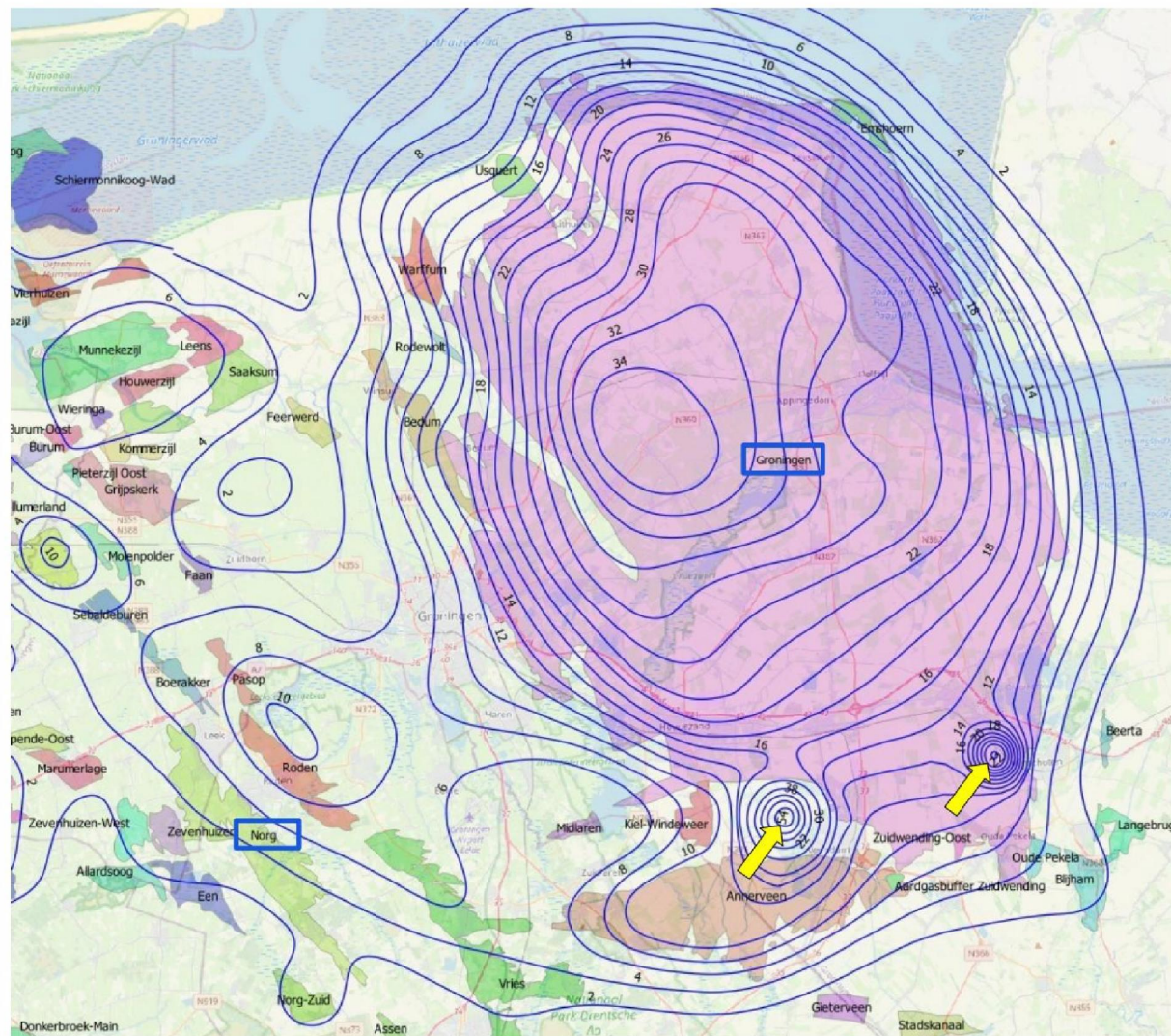
- Bodemdaling in 1995 door gasveld NORG (opgesteld door TNO, verstrekt door Deltares).
- 1 cm bodemdaling contourlijn op 1 oktober 2021 door enkel het Groningen gasveld (concept; opgesteld door TNO).



### 3. Wijze van opschonen

In onderstaande figuur zijn de gasvelden tezamen met de contourenlijnen van de bodemdaling eind 2018 weergegeven. Het Groningen veld is weergegeven in roze en de NORG gasopslag in geel.

Ten gevolge van zoutwinning treedt op 2 locaties eveneens bodemdaling op. Deze gebieden zijn aangeduid met een gele pijl. De westelijk gelegen zoutwinning betreft "Veendam". Oostelijk daarvan ligt "Westerlee".



Figuur: Ligging gasvelden en gemeten bodemdaling in 2018



De bodemdaling bestaat uit:

- Daling door Groningen gasveld en gasopslag Norg
- Daling door overige kleine gasvelden
- Daling door andere mijnbouwactiviteiten waarvan de zoutwinning bij Veendam en Westerlee de belangrijkste zijn
- Natuurlijke bodemdaling door inklinking van de ondergrond

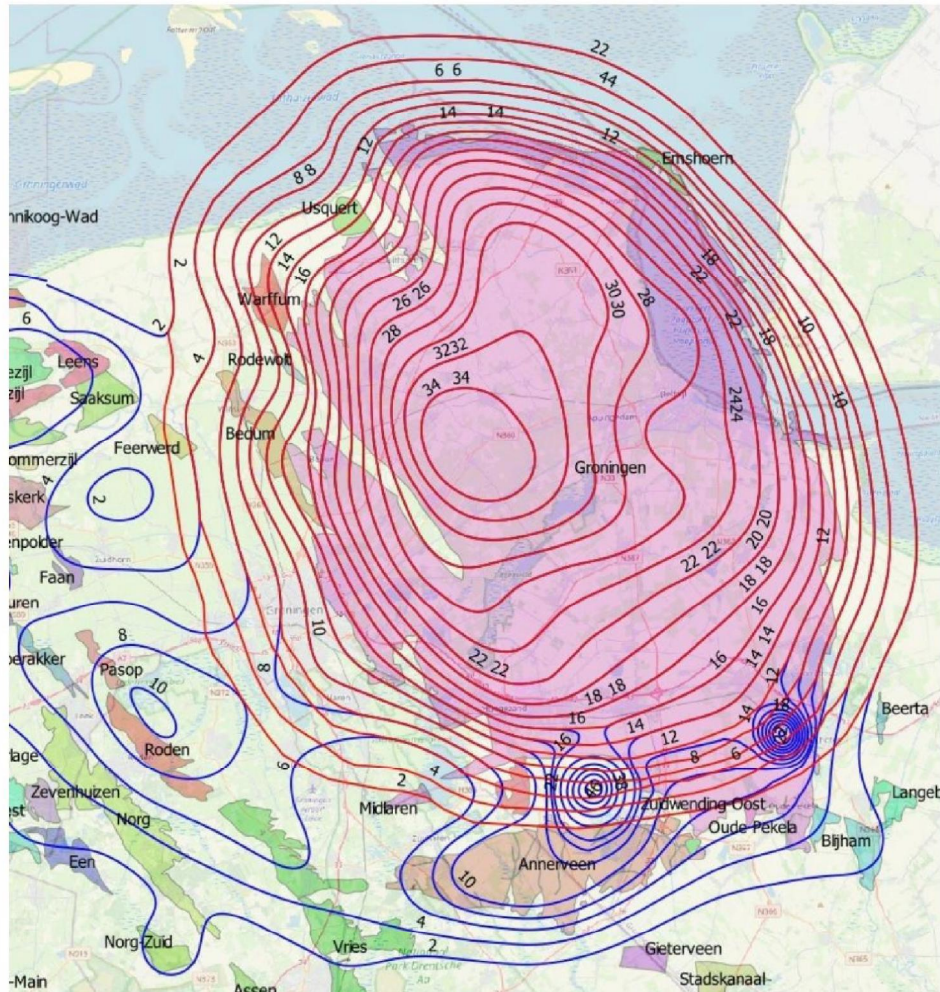
Uit de statusrapporten van de NAM blijkt dat men met behulp van diepe putten de natuurlijke bodemdaling in kaart wou brengen (verschil in bodemdaling op maaiveldniveau en op een diepte van een paar honderd meter). De resultaten lieten echter onderling grote verschillen zien en konden niet gebiedsgewijs worden toepast. Het in kaart brengen van de natuurlijke bodemdaling is derhalve door de NAM gestaakt.

Door de natuurlijke bodemdaling niet te verrekenen wordt de bodemdaling door de gaswinning van het Groningen veld en NORG overschat. Dit past bij het ruimhartige karakter van het IMG. Er zijn geen pogingen ondernomen om de natuurlijke bodemdaling rekenkundig in kaart te brengen en in mindering te brengen op de gemeten bodemdaling.

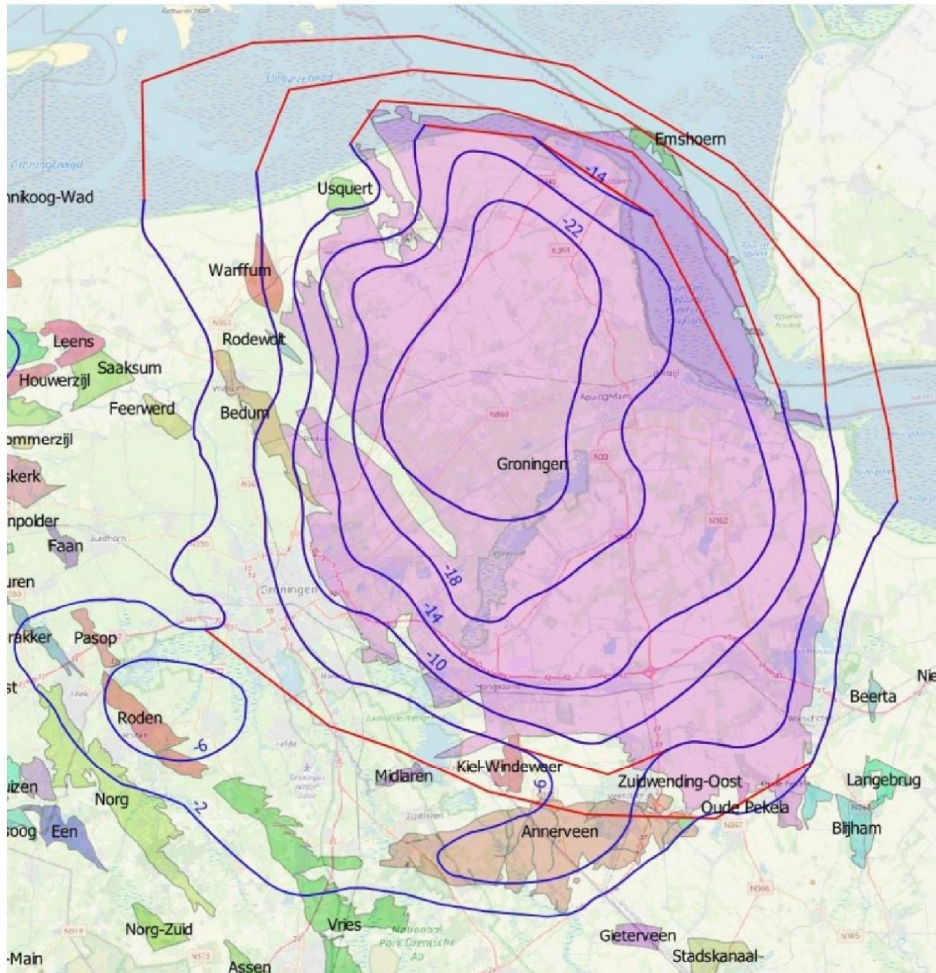
Aan de noord- en oostzijde bevinden zich (vrijwel) geen kleine gasvelden en daar vindt ook geen zoutwinning blijft. Deze contourlijnen hoeven derhalve niet aangepast (opgeschoond) te worden. Aan de west- en vooral aan de oostzijde is veel verstoring door andere gasvelden en zoutwinning. Opschoning heeft plaatsgevonden door de contourlijnen op plaatsen waar vrijwel geen verstoring is – op het oog - met elkaar te verbinden, waarbij globaal de contouren van het Groninger gasveld werden gevuld.

Bij gasopslag Norg is vanaf 1998 (het eerste jaartal waar de contourlijnen beschikbaar zijn) niet of nauwelijks nog sprake van bodemdaling of -rijzing. Wil IEDB mogelijk schade veroorzaken moet de bodemdaling of -rijzing ten minste 2 cm bedragen. Vanaf 1998 en later bedraagt, op basis van de beschikbare contourlijnen, de bodemdaling of -rijzing naar alle waarschijnlijkheid minder dan de grens van 2 cm. Aangegeven is naar alle waarschijnlijkheid, omdat ten noordoosten van NORG gasveld Roden ligt met een bodemaling van 10 cm in 2018. De bodemdaling van dit gasveld overlapt het invloedsgebied van Norg, waardoor de bodemdaling bij Norg niet goed te onderscheiden is. Omdat de invloed van Norg naar alle waarschijnlijkheid kleiner is dan de grens van 2 cm zijn derhalve geen contourlijnen opgesteld rondom gasopslag Norg (zie ook hoofdstuk 5).

De volgende figuren laten het resultaat van de opschoning zien voor de jaartallen 2018 en 2003.



Figuur: Ligging gasvelden en gemeten (blauw) en opgeschoonde (rood) bodemdaling 2018



Figuur: Ligging gasvelden en gemeten (blauw) en opgeschoonde (rood) bodemdaling 2003

Bij de resultaten van 2003 wordt opgemerkt dat de broninformatie alleen contourlijnen per 4 cm daling bevat. Hierdoor ontstaat een veel grover beeld in vergelijking met 2018 dat counterlijnen per 2 cm bodemdaling bevat. Daarnaast lopen de contourlijnen niet door ter hoogte van de Waddenzee en de Eems en Dollard. Voor numerieke redenen – ten behoeve van de interpolatie – is het echter wel noodzakelijk dat de contourlijnen gesloten zijn. Daarom zijn contourlijnen ter plaatse van de Waddenzee, Eems en Dollard alsnog met elkaar verbonden. Dit is vrij grof gedaan, maar heeft geen invloed op de IEDB analyse omdat zich hier geen peilvakken en gebouwen bevinden.



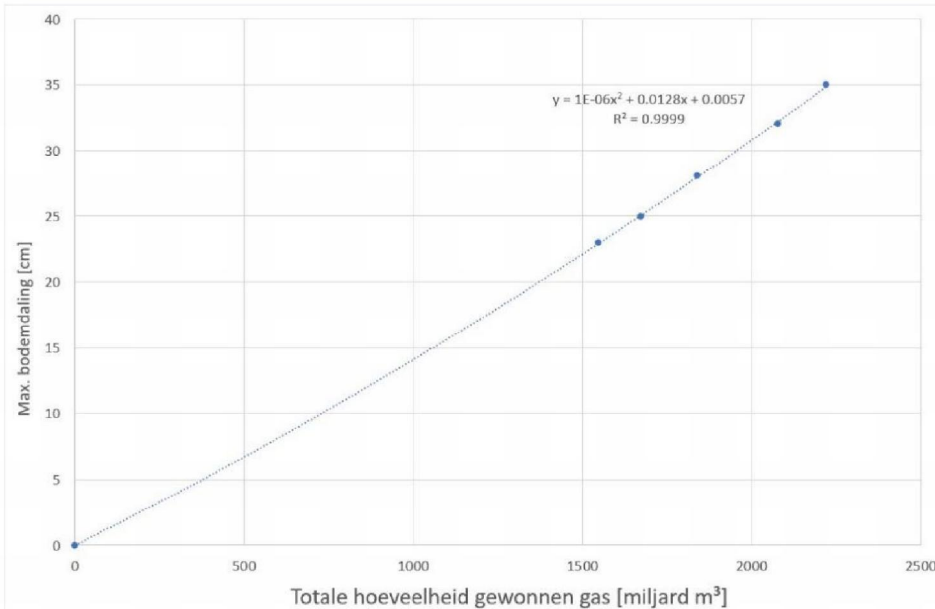
#### 4. Periode van start gaswinning tot 1998

Vanaf de periode van start gaswinning (1963) tot 1998 zijn geen contourlijnen beschikbaar als bronmateriaal. Voor de IEDB-analyse is echter wel inzicht benodigd in de opgetreden bodemdaling in deze periode.

Er is echter een duidelijke correlatie tussen de hoeveelheid gewonnen gas en de opgetreden bodemdaling. De jaarlijkse hoeveelheid gewonnen gas uit het Groningen gasveld is echter bekend en kan worden gedownload op de site van de NAM

([https://www.nam.nl/gas-en-olie/gaswinning.html#iframe=L2VtYmVkJ2NvbXBvb mVudC8\\_aWQ9Z2Fzd2lubmluZyN0YWItdGFjLWRvd25sb2Fkcy00ZmJmMTQ5OGNh MzY0YzEzOTg2ZGU5NjI5ZTJmYWFnNg](https://www.nam.nl/gas-en-olie/gaswinning.html#iframe=L2VtYmVkJ2NvbXBvb mVudC8_aWQ9Z2Fzd2lubmluZyN0YWItdGFjLWRvd25sb2Fkcy00ZmJmMTQ5OGNh MzY0YzEzOTg2ZGU5NjI5ZTJmYWFnNg)).

Verondersteld is dat invloedsgebied van het Groningen gasveld min of meer constant blijft (de buitenste contour met 2 cm bodemdaling). Dit beeld wordt ook bevestigd indien alle beschikbare contourlijnen op elkaar worden gelegd. Vervolgens is de totale hoeveelheid ontrokken gas vergeleken met de maximaal opgetreden bodemdaling in de jaren 1998, 2003, 2008, 2013 en 2018. Deze relatie (formule) is weergegeven in onderstaande figuur.



Figuur: Relatie tussen totale hoeveelheid gewonnen gas en opgetreden bodemdaling

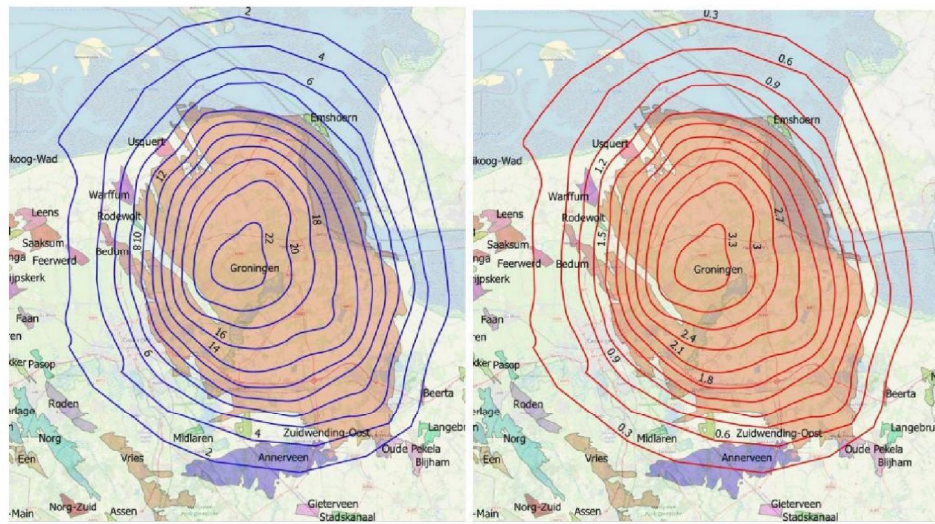


Met deze relatie is vervolgens aan de hand van de totale hoeveelheid gewonnen gas de bodemdaling bepaald. Vervolgens is een schalingsfactor bepaald (zie onderstaande figuur) door de bodemdaling in 1998 op 1,0 te stellen en in 1963 (start gaswinning) op 0,0. Vervolgens zijn van de jaren 1973, 1978, 1983, 1988 en 1993 contourlijnen bepaald, door de opgeschoonde contourlijnen van 1998 te vermenigvuldigen met de schalingsfactor.

Bewerking data:	Jaar totaal	Cumulatief	Max. bodemdaling [cm]	Schalingsfactor	
				Bodemdal (functie)	t.o.v. 1998
1963	1,894,120.00			0.0	0.00
1964	0.00	1,894,120.00		0.0	0.00
1965	866,234,160.00	866,128,280.00		0.0	0.00
1966	3,369,918,940.00	4,238,047,220.00		0.1	0.00
1967	6,904,629,660.00	11,142,676,880.00		0.1	0.01
1968	14,599,062,950.00	25,741,739,830.00		0.3	0.01
1969	23,156,740,010.00	48,898,479,840.00		0.6	0.03
1970	34,256,732,580.00	83,155,212,420.00		1.1	0.05
1971	47,337,630,050.00	130,492,842,470.00		1.7	0.07
1972	60,377,076,750.00	190,869,919,220.00		2.5	0.11
1973	70,696,368,430.00	261,566,287,650.00		3.4	0.15
1974	82,419,451,690.00	343,985,739,340.00		4.6	0.20
1975	84,047,180,960.00	428,032,920,300.00		5.7	0.25
1976	87,735,968,400.00	515,768,888,700.00		6.9	0.30
1977	83,313,058,021.63	599,081,946,721.63		8.1	0.36
1978	83,313,058,021.63	682,395,004,743.26		9.3	0.41
1979	72,168,483,750.59	754,563,488,493.85		10.4	0.45
1980	65,043,799,600.00	819,607,288,093.85		11.4	0.50
1981	59,052,756,803.00	878,660,044,896.85		12.2	0.54
1982	48,369,313,768.00	927,029,358,664.85		13.0	0.57
1983	50,056,334,513.00	977,085,693,177.85		13.7	0.60
1984	49,807,115,976.00	1,026,892,809,153.85		14.5	0.63
1985	51,907,454,053.00	1,078,800,263,206.85		15.3	0.67
1986	41,546,240,332.64	1,120,346,503,539.49		16.0	0.70
1987	39,066,454,092.30	1,159,412,957,631.79		16.6	0.72
1988	30,341,588,082.53	1,189,754,545,714.32		17.1	0.75
1989	27,880,196,683.98	1,217,634,742,398.30		17.5	0.76
1990	29,067,338,168.31	1,246,702,080,566.61		18.0	0.79
1991	38,580,239,447.47	1,285,282,320,014.07		18.6	0.81
1992	41,510,109,310.58	1,326,792,429,324.66		19.3	0.84
1993	43,107,761,007.47	1,369,900,190,332.13		20.0	0.87
1994	34,510,194,932.40	1,404,410,385,264.54		20.5	0.90
1995	34,097,162,456.74	1,438,507,547,721.28		21.1	0.92
1996	42,135,542,853.83	1,480,643,090,575.11		21.8	0.95
1997	34,700,378,031.14	1,515,343,468,606.25		22.4	0.98
1998	30,922,705,836.21	1,546,266,174,442.46	23	22.9	1.00

Figuur: Schalingsfactor t.o.v. referentiejaar 1998

In de volgende figuur zijn de aldus bepaalde opgeschoonde contourlijnen van 1973 weergegeven. Voor 1973 bedraagt de schalingsfactor x0,15. De contourlijn met een bodemdaling van 22 cm in 1998 bedraagt  $22 \times 0,15 = 3,3$  cm in 1973.



Figuur: Contourlijnen 1998 (links); contourlijnen 1973 (rechts) =  $1998 \times 0,15$



## 5. Vergelijk met later ontvangen data en inzichten

Deltares heeft in een eerder stadium onderzoek gedaan naar de effecten van de gaswinning bij Norg. Hierbij heeft TNO aan de hand van reservoirmodellen de maximale bodemdaling bij gasveld Norg bepaald. De daling was maximaal in 1995. Daarna is de bodemdaling deels weer teniet gedaan door gas op te slaan in het voormalige gasveld.

In de IEDB-analyse zijn voor gasopslag Norg dezelfde TNO-gegevens gehanteerd. Voor gasopslag Norg is derhalve geen gebruik gemaakt van opgeschoonede contourlijnen.

Door TNO is de 1 cm bodemdalingcontourlijn (bodemdalingscontourlijn op 1 oktober 2021) aangeleverd voor het Groningen gasveld. In onderstaande figuren wordt deze 1 cm bodemdalingcontourlijn vergeleken met de contourlijnen in 2018, 2003 en 1998. Hierbij is het gebied binnen de 1 cm bodemdalingcontour in groen weergegeven en de opgeschoonede contourlijnen in blauw.



*Figuur: Gebied binnen 1 cm bodemdalingcontourlijn 10-2021 TNO (groen) vs. opgeschoonede contourlijnen 2018 (blauw)*



Figuur: Gebied binnen 1 cm bodemdalingscontourlijn 10-2021 TNO (groen) vs. opgeschoonede contourlijnen 2003 (blauw)

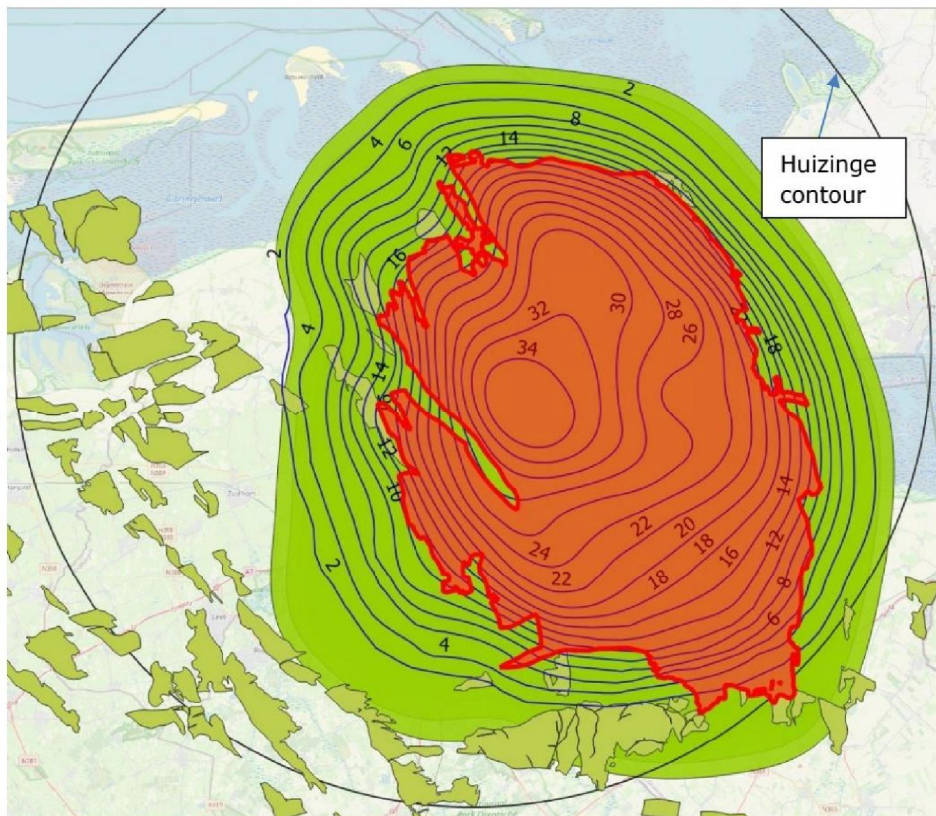


Figuur: Gebied binnen 1 cm bodemdalingscontourlijn 10-2021 TNO (groen) vs. opgeschoonede contourlijnen 1998 (blauw)



Bij de opgeschoonde contourlijnen 2018 valt op dat het invloedsgebied van de gaswinning onvoldoende ver in zuidelijke en zuidwestelijke richting is doorgezet indien deze worden vergelijk van de door TNO verstrekte 1 cm contourlijn. De opgeschoonde contourlijnen van 1998 en 2003 lijken beter aan te sluiten.

Om te kunnen beoordelen wat de invloed is van het onvoldoende doorzetten in zuidelijke en zuidwestelijke richting (opgeschoond contourlijnen 2018), is de zogenaamde Huizinge contour (trillingssnelheid 2 mm/s) ook nog toegevoegd aan de plot plus de gasvelden. Immers beperkt deze IEDB-analyse zich tot het gebied binnen de Huizinge contour. Het gebied daarbuiten is immers reeds door Deltares geanalyseerd (de 2 "lobjes").

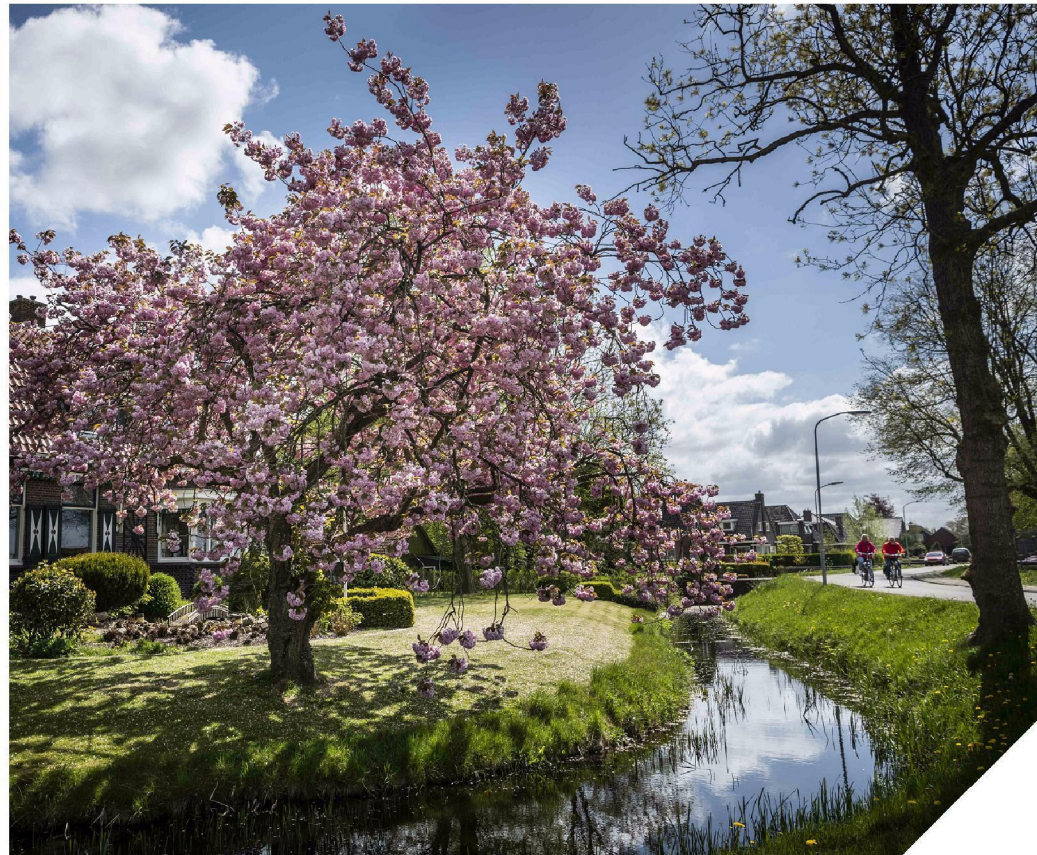


*Figuur: Situatie 2018: gasvelden (Groningen = rood), Huizinge contour, 1 cm contour, opgeschoonde contourlijnen*

Het gedeelte aan de zuidoost-zijde dat uitsteekt buiten de Huizinge contour is reeds door Deltares beschouwt. Direct daarboven liggen de contourlijnen nu dichter op elkaar. Hierdoor is het risico op IEDB in dit gebied groter. Aan de zuidzijde en zuidwest zijde is de bodemdaling net ver genoeg doorgezet. In deze gebieden wordt het IEDB-risico onderschat, daarboven juist weer iets overschat.

# INHOUD BEA

2 oktober 2023



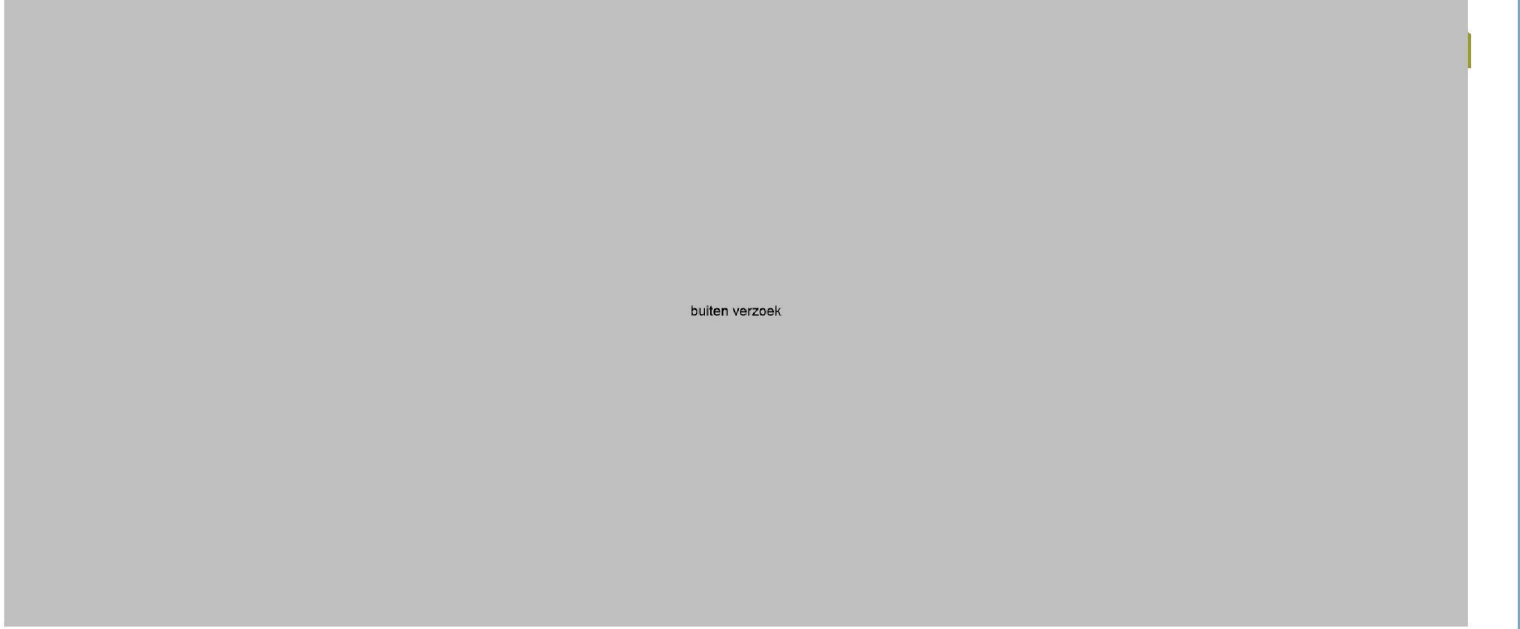
# Inhoud werksessie 2



- Conclusies vorige keer (incl. doorgeschoven vragen)

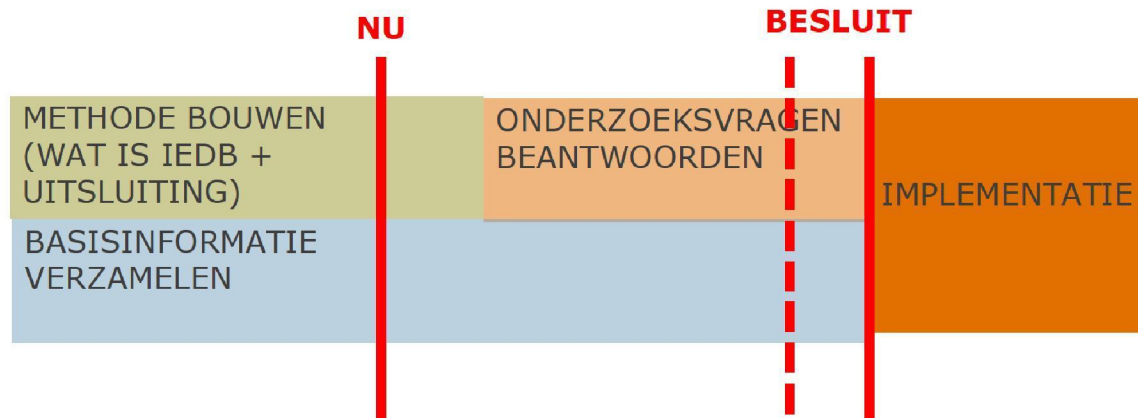
## Buiten verzoek

- Waarom 'doen' we IEDB / relatie met PEAG?
- Inventarisatie onderzoeks vragen
- Onderzoeks vragen toetsen aan onderzoeken (gaan die antwoord geven?)
- Afspraken voor vervolg

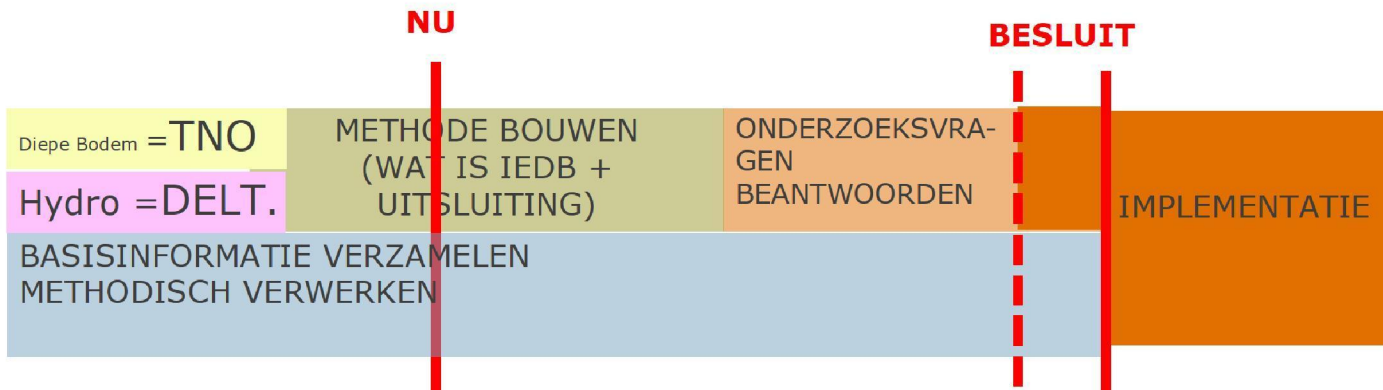


buiten verzoek

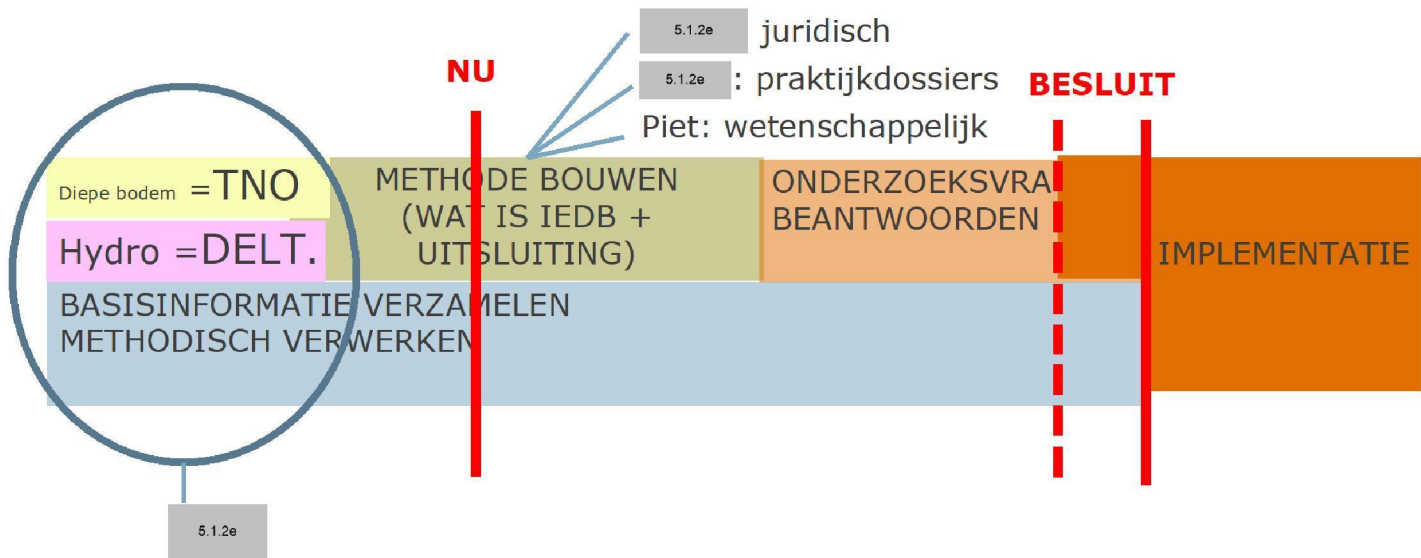
# Conclusies werksessie 1



# Conclusies werksessie 1



# Conclusies werksessie 1



# Conclusies werksessie 1

3.

5.2

## A. Bodemdaling (= TNO):

- [redacted] 5.2
- De bijlage bij hun rapport is zeer kritisch over de aanpak van IMG.
- De bodemdaling kent soms een onnauwkeurigheid van wel 20 cm. Hoe verhoudt zich dat met de zekerheid die we vanuit de hydrologie zoeken?

## B. Hydrologisch (= Deltares):

- We zoeken (lokaal) zekerheid op 2cm peilverandering. Dat is niet meetbaar. Daarnaast is algemeen gangbaar om 5cm als ondergrens te hanteren. Is er draagvlak in Nederland voor 2 cm?
- De conclusies van Deltares laten ruimte voor aanscherping. Daarmee is er interpretatieruimte in de conclusies?
- De studie is alleen bedoeld voor de lobjes Norg en Winschoten en niet voor het hele effectgebied.

# Conclusies werksessie 1



## C. Verwerking peilbesluiten (= IEDB Basis / Deltares)

- Wij leggen een verantwoordelijkheid (selectie relevante peilbesluiten) bij de waterschappen, die zij niet accepteren.
- Er zitten hiaten in het werk van IMG.
- IEDB-basis is niet altijd realistisch naar zeggen waterschappen / Commissie Bodemdaling.
- Er komen verschillende kaarten in omloop met daarin de effecten van peilveranderingen door mijnbouw. Hierin schuilen communicatie en juridische risico's.

## 4. Algemene opmerkingen bij de onderzoeken tot nu toe:

- We zijn in alle onderzoeken conservatief (bodemdalings-, hydrologisch, IEDB-basis). Een (bestuurlijke) afweging van hoe conservatief IMG moet zijn mist. Een analyse naar of deze stapeling nog redelijk is, is wenselijk.
- De onderzoeken lijken vaak op zich te staan en er is veel overgelaten aan interpretatie van onze opdrachtnemers. IMG heeft sommige keuzes (zoals de rol van de waterschappen) niet op het juiste niveau gemaakt.

# Conclusies werksessie 1

5. IMG is sterk afhankelijk van de kennis en inzet van TNO.  


5.2                            5.2
6. Juridisch zijn er een aantal denkrichtingen voor de (juridische) afhandeling van IEDB schade. Uitvoering geven aan deze denkrichtingen zal de deskundigen veel tijd kosten. Het is een bestuurlijke keuze of we de denkrichting willen of niet.
7. Wellicht dat het onderzoek van Piet/Jan aanleiding kan zijn om de uitgangspunten van Deltares ter discussie te stellen (daarvoor is dan waarschijnlijk nog wel een extra actie / onderzoeksraag aan Deltares nodig).

# Conclusies werksessie 1

8. De wetenschappelijke analyse is leidend in beantwoording van de vraag voor hoeveel objecten we IEDB kunnen uitsluiten. Het onderzoek van 5.1.2e (100+ praktijkdossiers) is ter validatie en om aan te tonen dat we de problematiek niet onderschatten. Daarmee is er minder sprake van interactie tussen de twee onderzoekssporen, dan eerder aangenomen.
9. IMG moet nog keuzes maken voor wat zij tot de autonome ontwikkelingen rekent en daarmee hoe 'erg' de peilverandering ten gevolge van mijnbouw is ten opzichte van andere peilveranderingen.

# B vanuit en voor oog op perspecti

1-2023

5.1.2e



# Definitie dienstverlening

buiten verzoek

# Waarom denken vanuit de aanvrager?

buiten verzoek

## Een Aanvrager is een Burger, Bewoner en een Mens

buiten verzoek

buiten verzoek

Instituut  
Mijnbouwschade  
Groningen



# Waarom denken vanuit de aanvrager?

buiten verzoek

# Project dienstverlening

buiten verzoek

## Werken vanuit klant(aanvrager)waarde

buiten verzoek

buiten verzoek

Instituut  
Mijnbouwschade  
Groningen



# Segmenteren op doenvermogen

buiten verzoek